

## Velocity Field Derived from Taiwan Continuous GPS Array (2007 - 2013)

Min-Chien Tsai<sup>1,\*</sup>, Shui-Beih Yu<sup>2</sup>, Tzay-Chyn Shin<sup>3</sup>, Kai-Wen Kuo<sup>1</sup>, Peih-Lin Leu<sup>1</sup>, Chien-Hsin Chang<sup>1</sup>, and Mei-Yi Ho<sup>1</sup>

<sup>1</sup> Seismological Center, Central Weather Bureau, Taipei, Taiwan, R.O.C.

<sup>2</sup> Institute of Earth Sciences, Academia Sinica, Taipei, Taiwan, R.O.C.

<sup>3</sup> Central Weather Bureau, Taipei, Taiwan, R.O.C.

Received 6 October 2014, revised 18 May 2015, accepted 21 May 2015

### ABSTRACT

Data were collected from 281 Taiwan continuous Global Positioning System (cGPS) Array sites from 2007 - 2013 and processed with GAMIT/GLOBK software. Power spectral density stacking from cGPS position time series in Taiwan found the spectral index as -0.72, -0.77, and -0.57 for the E, N, U components, respectively. This indicates the cGPS data errors can be described as a combination of white noise and flicker noise. The common-mode errors are removed by stacking data from 50 cGPS sites with data periods greater than 5 years. By removing the common-mode errors the GPS data precision is further improved to 2.3, 1.9, and 6.9 mm in the E, N, U components, respectively. After strict data quality control, time series analysis and noise analysis, we derive a new Taiwan velocity field using cGPS data from 2007 - 2013. The general pattern of the newly derived 2007 - 2013 velocity field is quite similar to that from previous studies, but the station density is much larger and spatial coverage better. About 80 mm yr<sup>-1</sup> plate convergence rate is observed, half of the rate is accommodated on the fold and thrust belt of western Taiwan and another half is taken up in the Longitudinal Valley and Coastal Range in eastern Taiwan. The velocities in western Taiwan generally show a fan-shaped pattern, consistent with the maximum compression tectonic stress direction. In northern Taiwan the velocity vectors reveal clockwise rotation, indicating the on-going extensional deformation related to the back-arc extension of the Okinawa Trough. In southern Taiwan, the horizontal velocity increases from about 40 mm yr<sup>-1</sup> in the Chia-Nan area to 55 mm yr<sup>-1</sup> in the Kao-Ping area with a counterclockwise rotation.

Key words: GPS, Time series analysis, Velocity field, Crustal deformation

Citation: Tsai, M. C., S. B. Yu, T. C. Shin, K. W. Kuo, P. L. Leu, C. H. Chang, and M. Y. Ho, 2015: Velocity field derived from Taiwan Continuous GPS Array (2007 - 2013). *Terr. Atmos. Ocean. Sci.*, 26, 527-556, doi: 10.3319/TAO.2015.05.21.01(T)

### 1. INTRODUCTION

Taiwan is situated in an active tectonic region with numerous thrust faults and folds due to on-going collision between the Luzon arc and Chinese continental margin. Numerous devastating earthquakes with magnitudes greater than 6 have occurred since 1900. The oblique convergence of the Eurasian and Philippine Sea Plates started at the beginning of Late Miocene period (Ho 1976; Barrier and Angelier 1986; Huang et al. 2006).

The Global Positioning System (GPS) has become an efficient tool for studying active tectonics and geodynamics (Dixon 1991; Hager et al. 1991; Feigl et al. 1993). Utilizing satellite positioning techniques each station can provide

precise global coordinates for its antenna position which can be used to monitor the horizontal and vertical crustal movements at the site (Altamimi et al. 2002). We derived a velocity field using 2007 - 2013 data from 281 sites in the Taiwan continuous GPS (cGPS) Array. The instrumentation and status of the cGPS array, data quality control and data processing procedures are well described. After strict and careful data quality control, times series analysis, noise analysis and common-mode error correction, we obtained a more reliable velocity field with more realistic uncertainty from the GPS position time series optimal model parameters. The results provide important information on the present-day crustal deformation in the Taiwan area. Further studies on the relation between seismic activity and strain accumulation or release can be carried out (Dixon 1991; Bock 1994; Hudnut 1995; Segall and Davis 1997).

\* Corresponding author  
E-mail: minchyan@cwb.gov.tw

## 2. TAIWAN CGPS ARRAY

In order to investigate the relationship between seismic activity and crustal deformation in the Taiwan area, the Central Weather Bureau (CWB) established a cGPS network composed of 16 sites in 1994 - 1996. After the 1999 Chi-Chi earthquake, CWB increased the total number of cGPS stations to 150 sites from 2001 - 2005. In the meantime, several agencies in Taiwan, including the Institute of Earth Sciences, Academia Sinica (IESAS), Central Geological Survey (CGS), and Ministry of the Interior (MOI), also installed many cGPS stations in the Taiwan area. Data collected from 2007 - 2013 from a total of 281 cGPS stations operated by CWB, IESAS, and CGS are used in this study (Fig. 1).

All stations in the Taiwan cGPS array are equipped with dual-frequency geodetic Global Navigation Satellite Systems (GNSS) receivers and antennas. The sampling interval for data collection is either 30 or 1 sec. GPS data acquired at continuous stations are transferred to the central control system at main office by ADSL, wireless, or manual downloading. Some CWB cGPS stations are co-located with borehole broad-band seismic stations [e.g., I-Chu station (ICHU) and LONT] or borehole strainmeter sites (e.g., JSUI and NHSI). Furthermore, 77 cGPS stations are located within 1 km of a strong-motion seismic station. Thus, we can obtain coseismic displacements and ground motion from both GPS and seismic data at the same site. These data can therefore be used to compare high-rate GPS results with seismic wave observations.

## 3. DATA QUALITY CONTROL

Raw data from each station is converted to Receiver-INdependent-Exchange (RINEX) format. Sometimes RINEX files may give wrong information or format errors because of incorrect initial setup for receivers. The most common problems are illogical or garbled data format, incorrect receiver or antenna types. The Translation, Editing, and Quality Check (TEQC) software developed by UNAVCO (a non-profit university-governed consortium that facilitates geoscience research and education using Geodesy) is employed to fix these type of problems. TEQC can read original binary file format and output into RINEX common format. The program allows editing, modification, cut, and merge observational data and even reassign data sampling intervals. In addition, TEQC can also be used to check static and dynamic GPS observation data quality (Estey and Meertens 1999).

Most of the cGPS stations are located at relatively stable sites that exhibit little possibility of local movement and can be preserved for a long period of more than 10 years. Most sites have good sky visibility for elevation angles larger than 15 degrees. For example, the ICHU is a deeply anchored and braced monument station with very good data quality and sky visibility (Figs. 2a and 3). In Fig. 2a the ticks outside the

circle indicate the station's azimuth from 0 - 360°, 0° is in the north direction. Blue dots describe the path of the received satellites on that day from elevation 0 - 90°. The ICHU station sky-plots at the same day (May 31) in 2007 and 2013 reveal almost the same patterns and show good sky visibility (Fig. 2a). The proportion of ICHU receiving observations to predicted observations are 100 and 97% on May 31 in 2007 and 2013, respectively. Figure 2b shows the site photos taken toward the north, east, south, and west directions, respectively in 2013. The quality-control-time-series figure is another way to realize observation data qualities. Figure 3 presents the predicted and observed number of data (Fig. 3a), cycle slip numbers (Fig. 3b), and multipath errors for L1 and L2 (Fig. 3c) ICHU station. Basically, the ICHU site received more than 95% of the predicted number of observations. The multipath errors stay in the same level of less than 50 cm. Cycle slips occurred more frequently from 2010 - 2013, which might be due to intensive solar activity.

Another example, the Shan-Da-Thi station (DASI), was installed in 2005 on a hill near the east coast of Taiwan. Figure 4a shows the DASI station sky-plots for 31 May in 2007 and 2013, respectively. We can see better sky visibility in 2007 and that fewer satellite signals were received in 2013 due to bad sky visibility, suggesting that the local environment at this site changed dramatically. The proportion of receiving observations to predicted observations for DASI also decreased from 82 - 54% from 31 May in 2007 and on the same day in 2013. As is well known, data quality is usually relative to site sky visibility and good sky visibility comes from good site environment maintenance. Because the DASI site land owner grew trees near the antenna monument several years after the first installation, the surrounding tall trees explain the very bad sky visibility (Fig. 4b). Figure 5 presents observed data numbers (Fig. 5a), cycle slip numbers (Fig. 5b), and multipath errors of L1 and L2 (Fig. 5c) of DASI. The percentage of the total number of DASI received data is less than 60% (Fig. 5a) with a lot of cycle slips (Fig. 5b). Furthermore, multipath errors increased from 2007 - 2013 and reached a maximum value in 2013. All of the QC results from Figs. 4a and 5 are consistent with the site environment changes shown in Fig. 4b. Therefore, the routine sky-plot and quality control are very important, convenient tools for the cGPS operation.

## 4. DATA PROCESSING

All cGPS data were processed by GAMIT/GLOBK software v.10.4 (Herring et al. 2010) with standard procedures. GAMIT uses the least-squares method to process data, and then obtain the site coordinates from daily solutions. GAMIT contains 5 modules, including ARC, MODEL, AUTCLN, CFMRG, and SOLVE modules. GLOBK uses Kaman filter to get a combined solution of several subnets or periods (Dong et al. 1998).

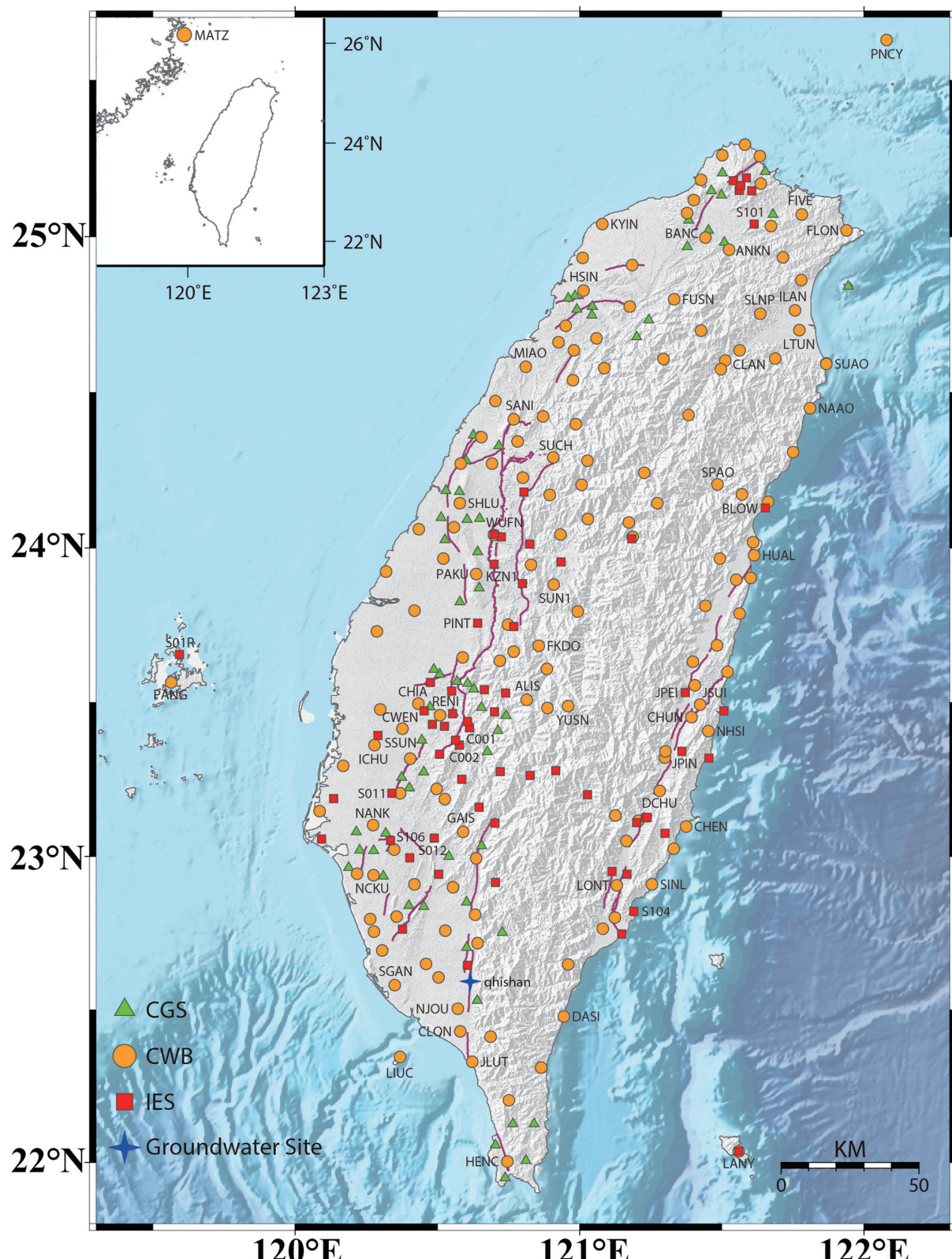


Fig. 1. Taiwan continuous Global Positioning System (cGPS) Array. The green triangle, yellow circle, and red square symbols indicate the cGPS sites operated by the Central Geological Survey (CGS), Central Weather Bureau (CWB), and Institute of Earth Sciences, Academia Sinica (IESAS), respectively. Pink lines are active faults.

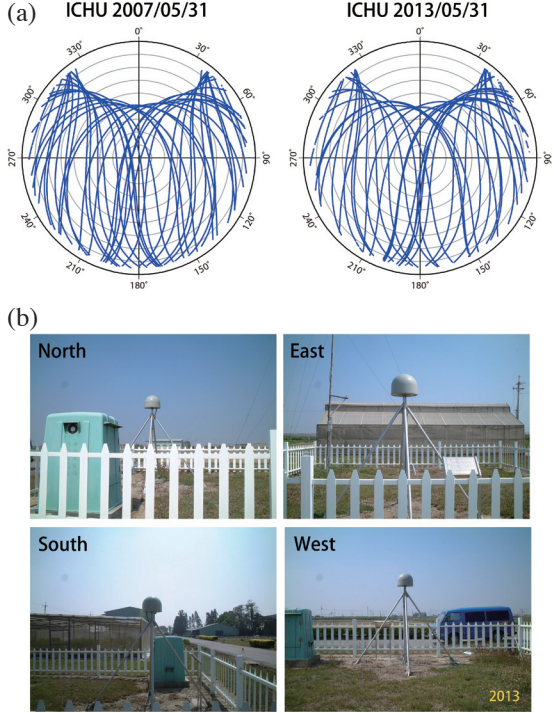


Fig. 2. (a) Sky plots of ICHU station on May 31, in 2007 and 2013, respectively. The ticks outside of circle indicate the station's azimuth from 0 - 360°, 0° is in the north direction. Blue dots describe the received satellites path at that day from elevation 0 - 90°. (b) Station photos taken toward the north, east, south, and west directions, respectively in 2013.

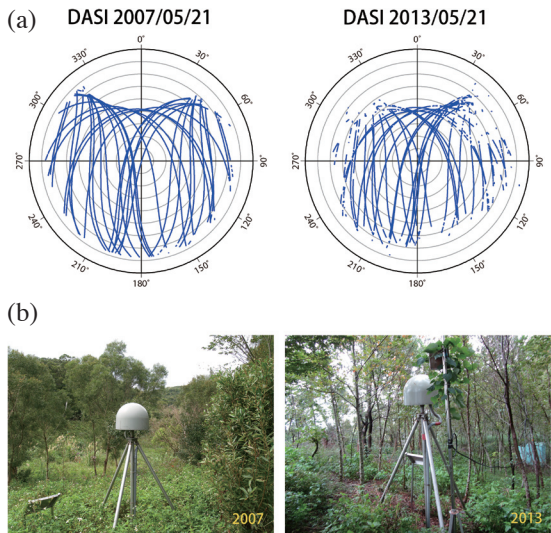


Fig. 4. (a) Sky plots of DASI station on May 31, in 2007 and 2013, respectively. The ticks outside of circle indicate the station's azimuth from 0 - 360°, 0° is in the north direction. Blue dots describe the received satellites path at that day from elevation 0 - 90°. (b) Station photos taken in 2007 and 2013, respectively.

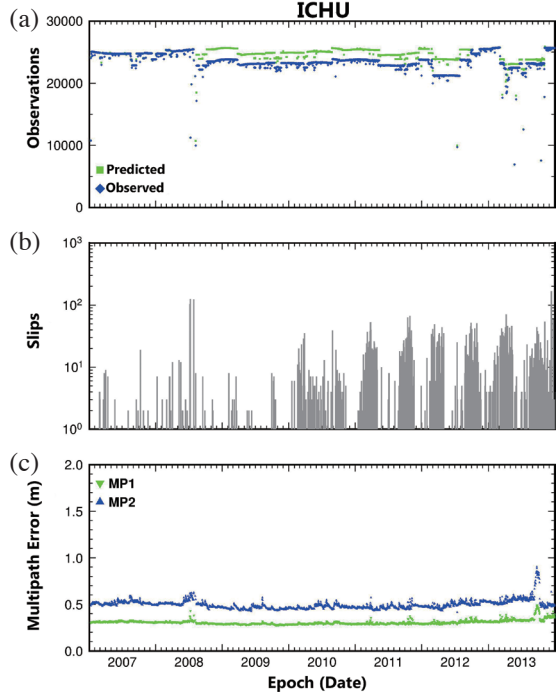


Fig. 3. The quality-control time series of ICHU station. (a) The green square and blue diamond symbols indicate predicted and observed number of observations, respectively. (b) Gray bars indicate number of cycle slip in logarithmic scale from 2007 - 2013. (c) The multipath errors, MP1 and MP2 on L1 and L2, respectively.

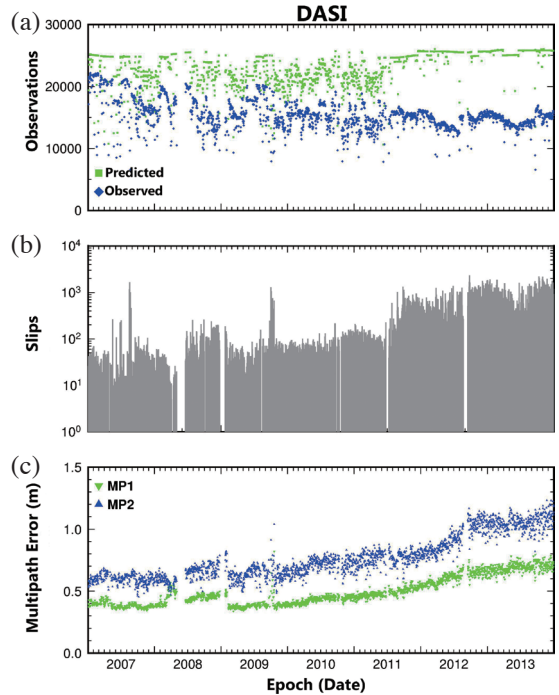


Fig. 5. The quality-control time series of DASI station. (a) The green square and blue diamond symbols indicate predicted and observed number of observations, respectively. (b) Gray bars indicate number of cycle slips in logarithmic scale from 2007 - 2013. (c) The multipath errors, MP1 and MP2 of L1 and L2, respectively.

The main GAMIT body functions and features are as follows: (1) ARC: ephemeris format conversion module, using partial differential to calculate orbit ephemeris. (2) MODEL: estimate theoretical value, the residual of observations and theoretical value will be considered as a reference parameter for the adjustment basis. (3) AUTCLN: fix cycle slip and correct model parameters. (4) CFMRG: generate the parameter configuration files. (5) SOLVE: solving equations. We first use the least-squares method to get the optimal model parameters and minimize residuals, then estimate the coordinates and orbital parameters of each station. These processes were generally executed 2 iterations (Fig. 6), and the normalized root-mean square value (NRMS) of the final results should be smaller than 0.25, otherwise we need to evaluate if any parameters are over-constrained in GAMIT processing.

Some GAMIT processing tables are very important and always need to be updated to maintain the correct information. For example: antenna mode table (antmod.dat), earth rotation parameters table (ut1., pole.), nutation table (nutabl.) ...etc. The GAMIT and GLOBK processing control files need to be setup correctly. The main control files are as follows: (1) sites.defaults: the list of sites used for each different subnet. (2) Process.defaults: file for setup computation environment, including reference frame, data sampling rate, orbit parameters and other information. We use International Terrestrial Reference Frame 2008 (ITRF2008) as the reference frame. (3) Sittbl.: site control file, setup constrain of coordinate and velocity for each station. (4) Sestbl.: session control table, setup all kinds of parameters and modules. We set the orbit constrain as “RELAX.” for loose orbit parameter constraint with an elevation cutoff angle of 15° to reduce any multipath effects and noises. We used the Vi-

enna Mapping Function 1 (VMF1) for troposphere correction parameters, which is developed by the Victoria Vienna team. VMF1 is based on GMF (global mapping function) which developed from a numerical weather model (NWM) estimated using more than 20 years weather data (Boehm et al. 2006). The VMF1 can use different weights for different zeniths to conduct more accurate tropospheric error correction. (5) Station.info: site information table, includes site name, site code, receiver type, antenna type, data time span, and antenna height. This table needs to be updated when a station has an instrument change. (6) Apr file: a priori site coordinate files, set all initial station coordinates for GAMIT processing. The initial coordinates cannot have large bias from the site coordinates solution, or it will make the processing crash. All of the control files used for GAMIT processing in this paper can be found at the Geophysical Database Management System (GDMS) website (<http://gdms.cwb.gov.tw/index.php>) of CWB.

Usually we obtain loosely constrained parameter estimates and covariance solution files from the GAMIT processing results. These data are then passed to GLOBK for data combination to estimate station coordinates and velocities and orbital and Earth-rotation parameters (Feigl et al. 1993; Dong et al. 1998). GLOBK contains three major modules, globk, glred, and glorg. The functions of three modules are as follows: (1) globk: used for data combination in time domain or space domain. In other words, globk can combine decades of data into one solution, or merge the number of subnets into a daily solution, also estimate the site coordinates or velocity at the same time. It outputs four kinds of files, they are \*.gcr (constrained, bias free solution), \*.gcx (constrained, bias fixed solution), \*.glr (loose,

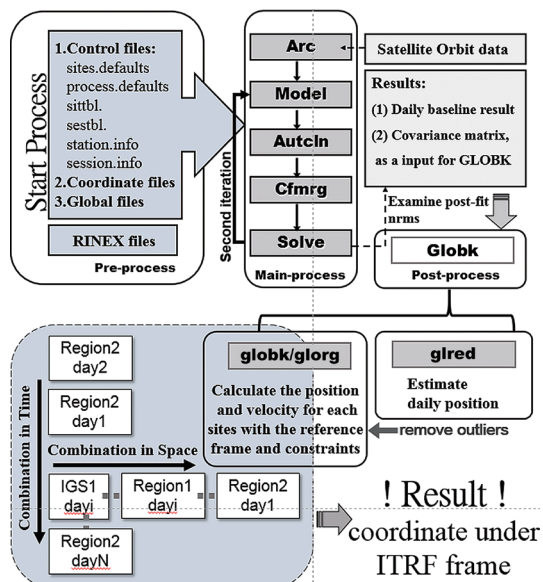


Fig. 6. GAMIT/GLOBK data processing flow chart. Including three parts, the pre-process and main-process for GAMIT part, and post-process for GLOBK part. Each section has its own main modules, input files and output files.

bias free solution), and \*.glx (loose, bias fixed solution). These files can be used for different purposes. (2) Glred: used for repeatability analysis. The major program is similar to globk, but glred takes the daily solution as independent and makes prominent of coordinate repeatability. (3) Glorg: merge GAMIT solution to get optimal coordinates by rotation, translation, and scaling. There are three steps in GLOBK processing (Fig. 6): (1) use glred first to obtain daily solution and time series of each site and remove outliers. (2) Without outliers, use globk/glorg to merge all solutions and estimate the optimal coordinates and velocities for each site. We use a loose constraint in this step to ensure that glorg has enough room to perform adjustment on rotation, translation and scaling. (3) Finally, glorg is used again to define a reference frame with tight constraints to achieve the optimal ITRF2008 coordinates. The International Terrestrial Reference System (ITRS) is realized and maintained by the International Earth Rotation and Reference Systems Service (IERS). The ITRS realization, through the International Terrestrial Reference Frame (ITRF) is updated regularly to take into account new accumulated data and also improved analysis strategies applied by the analysis centers of the contributed techniques. ITRF2008 is a refined version of the ITRF based on reprocessed solutions for the four space geodetic techniques: Very Long Baseline Interferometry (VLBI), Satellite Laser Ranging (SLR), GNSS, and Doppler Orbitography Radiopositioning Integrated by Satellite (DORIS), spanning 29, 26, 12.5, and 16 years of observations, respectively (Altamimi et al. 2011).

We processed a total of 281 Taiwan cGPS stations with time periods longer than 1.5 years and 25 International GNSS Service (IGS) stations. The precise IGS final orbits are used in the processing. Considering the computing capability and limitations of the number of sites for each subnet in GAMIT, we divided the 281 Taiwan cGPS stations into 12 sub-networks. In order to constrain the Taiwan subnet solution to the ITRF2008 reference frame, an additional 25 IGS station subnet was also used (Fig. 7). In order to connect all subnets we choose 5 local sites with longer data time span and good quality as common stations for all subnets. These common sites are S01R (Paisha, Penghu), S101 (Nankang, Taipei), S104 (Fushan, Taitung), LANY (Lanyu, Taitung), and HENC (Henchun, Pingtung) (Fig. 1).

We choose 18 IGS sites with good data quality and longer time span in the Asia-Pacific region as reference stations for use in GLOBK processing stabilization (Fig. 7). Another 7 IGS sites in the same region were incorporated in the processing for better connection between IGS sites. The 18 IGS sites used for stabilization are: COCO (Cocos Island, Australia), DAEJ (Daejeon, Korea), DARW (Darwin, Australia), DGAR (Diego Garcia Island, United Kingdom), FAIR (Fairbanks, Alaska, U.S.A.), GUAM (Guam, U.S.A.), HOB2 (Hobart, Australia), IISC (Bangalore, India), IRKT (Irkutsk, Russia), KOKB (Kauai, Hawaii, U.S.A.), KUNM

(Kunming, China), LHAZ (Lhasa, Tibet, China), PERT (Perth, Australia), SHAO (Shang-hai, China), TOW2 (Townsville, Australia), THTI (Tahiti, French Polynesia), TSKB (Tsukuba, Japan), and WUHN (Wuhan, China). In addition, TSKB was not used for stabilization after 11 March 2011 off-Tohoku earthquake ( $M_w$  9.0) to avoid the impact of post-seismic deformation. The coordinates, velocities and time-series of IGS sites can be found at IGS or SOPAC (Scripps Orbit and Permanent Array Center) websites (<http://www.igs.org/>; <http://sopac.ucsd.edu/>).

The loosely constrained daily solutions from 13 GAMIT subnets are combined and constrained into the ITRF2008 reference frame through IGS station stabilization in GLOBK to obtain the precise position time series for each site. The coordinate constraints for 18 stabilization IGS stations are 5, 5, and 10 cm on X, Y, Z components, respectively, to avoid over-constraining in GLOBK processing. The correlation statistics between the solution precision and number of stabilization sites point out that the daily solution will usually be an outlier if less than 4 sites are used in GLOBK stabilization. This could be because GLORG needs at least 4 stabilization sites to adjust the optimal network geometry using translation, rotation and scaling. Figure 8 shows the statistics for 18 IGS sites used in GLOBK stabilization. The black, cyan and yellow color bars indicate RINEX archive data used in GAMIT, and the data used in GLOBK for stabilization, respectively. We can see that TSKB has long and complete raw-data and GAMIT solutions from 2007 - 2013, but we do not use it for stabilization after the 11 March 2011 off-Tohoku earthquake. The FAIR, KOKB, and THTI sites are frequently excluded in stabilization due to their long baselines. Figure 9 is the statistics for the number of sites used in GLOBK stabilization from 2007 - 2013. It reveals the minimal number of used sites is 8 in May 2012, and less than 10 days with only 9 stabilization sites. Twelve to seventeen sites are used for stabilization during the study period, suggesting the daily solutions are well constrained on the ITRF2008 reference frame.

## 5. GPS TIME SERIES ANALYSIS

### 5.1 Pre-Processing and Time Series Analysis

The velocity of each cGPS site is estimated from the position time series through a model that removes outliers and systematic errors. We transform the coordinates from ITRF2008 Cartesian coordinates into ENU (east, north, and up components) coordinates for easier site movement understanding in geophysical applications. The outliers need to be removed before time series analysis. All outliers were removed using the standard deviation (STD) and moving-average method (MA). The STD represents a mean data series values trend and most outliers can be easily removed using 3.5 times STD. For some special cases, e.g., the large offset caused by coseismic displacement or instrument change, the STD method may not work well because offsets

will enlarge the STD value and reduce the capability of removing outliers. Therefore, combining STD with the MA method can make outlier removal complete. For the 7 years (2007 - 2013) long GPS data the optimal window size is 30 days and shifts every 10 days. More than 98% of the 281 cGPS position time series had a removed outlier percentage less than 3% for whole data period. Nine percent of the 281 cGPS only removed less than 1% outliers, which means very good data quality, like the ICHU station (Fig. 10). Only a few sites presented large scattered position time series. For example, the DASI and FKDO stations show large scattered data distribution after the middle of 2011 caused by worse sky visibility (Figs. 11 and 12).

The velocity of each cGPS site is estimated from the

position time series through a model as follows (Nikolaidis 2002):

$$y(t_i) = a + bt_i + c \sin(2\pi t_i) + d \cos(2\pi t_i) + e \sin(4\pi t_i) + f \cos(4\pi t_i) + \sum_{j=1}^{n_g} g_j H(t_i - T_{gj}) + \sum_{j=1}^{n_h} h_j H(t_i - T_{hj}) t_i + \sum_{j=1}^{n_k} k_j \exp[-(t_i - T_{kj})/\tau_j] H(t_i - T_{kj}) + v_i \quad (1)$$

Where  $t_i$  for  $i = 1, \dots, N$  are the daily solution epochs in units of years, and  $H$  is the Heaviside step function. The first two terms are the site position,  $a$ , and linear rate,  $b$ , respectively. Coefficients  $c$  and  $d$  describe the annual periodic motion, while  $e$  and  $f$  describe semi-annual motion. The next term

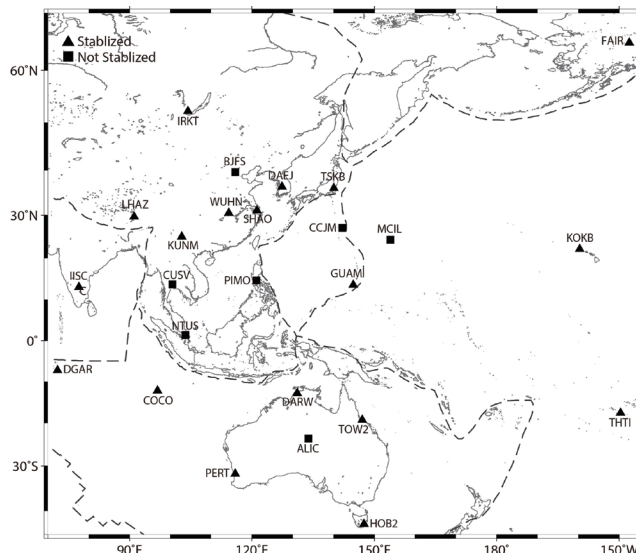


Fig. 7. Distribution of IGS stations used in GAMIT/GLOBK processing. The triangular indicates the stabilization sites used in GLOBK, and the square represents the IGS sites only used in GAMIT processing. Black dash line denotes plate boundaries.

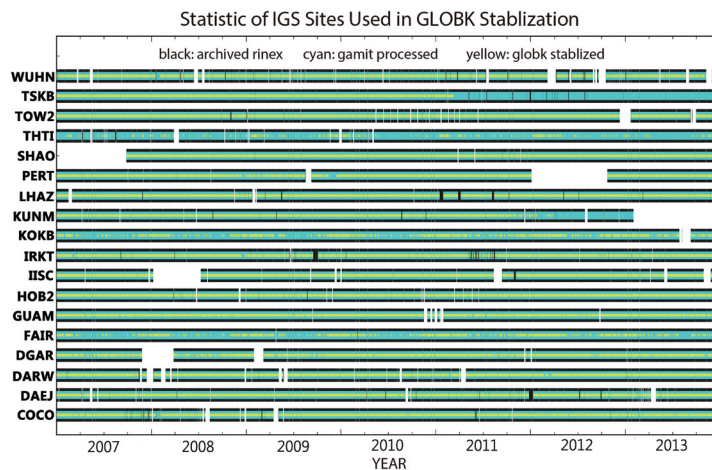


Fig. 8. The statistics of 18 IGS sites used in GLOBK stabilization. The horizontal axis represents the data time span and vertical axis indicates the names of 18 IGS sites. The black, cyan and yellow color bars indicate RINEX data of archive, data used in GAMIT, and data used in GLOBK, respectively.

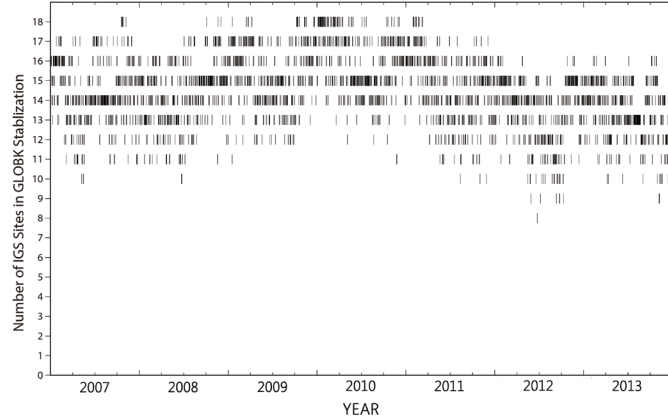


Fig. 9. The statistics for the number of sites used in GLOBK stabilization from 2007 - 2013.

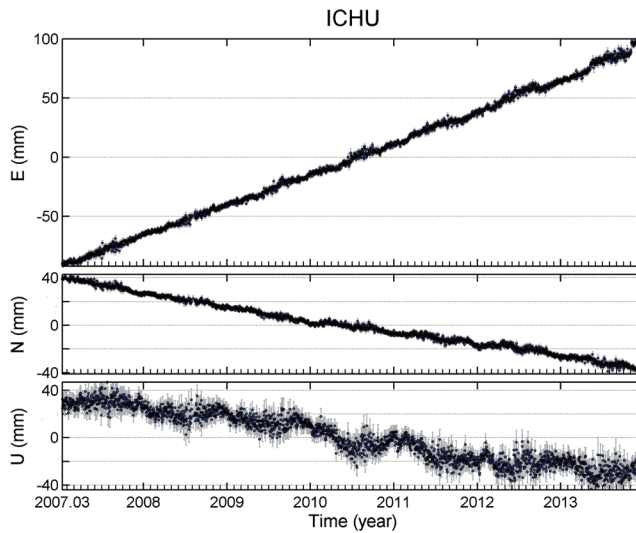


Fig. 10. GPS position time series of ICHU station, in the east, north and up components, respectively. The black solid circles and light gray bars indicate the observed daily solutions and their formal errors, respectively.

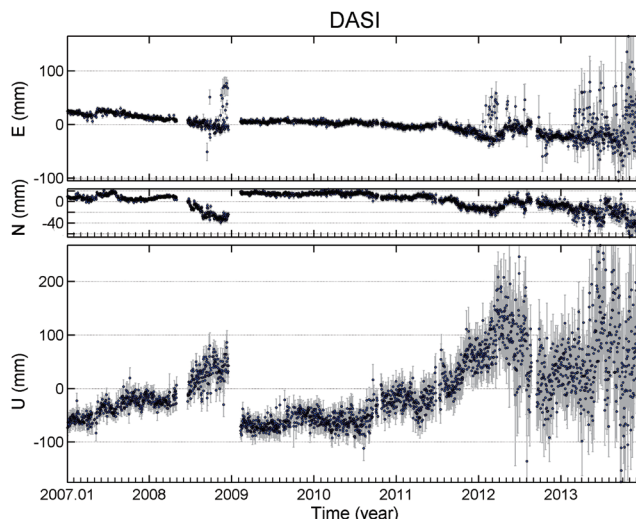


Fig. 11. GPS position time series of DASI station in the east, north and up components, respectively. The black solid circles and light gray bars indicate the observed daily solutions and their formal errors, respectively.

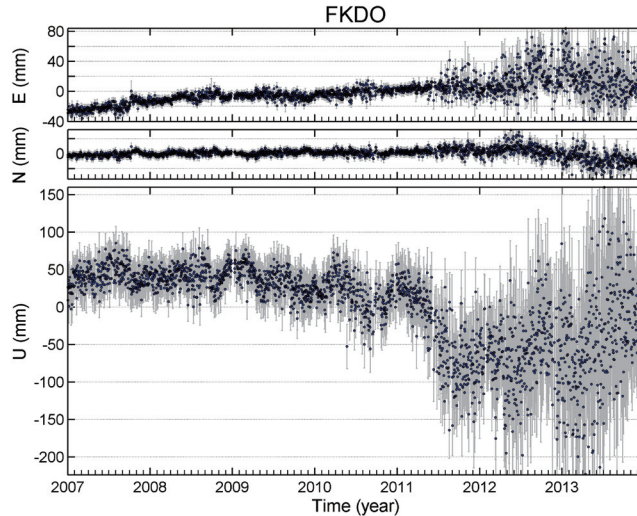


Fig. 12. GPS position time series of FKDO station in the ENU, respectively. The black solid circles and light gray bars indicate the observed daily solutions and their formal errors, respectively.

corrects for any number ( $n_g$ ) of offsets, with the magnitudes  $g$  and epochs  $T_g$ . The coefficients  $h_j$  and  $k_j$  are used for the post-seismic rate change and post-seismic exponential decay description with the relaxation time  $\tau_j$ , respectively. The final term  $v_i$  is the model residual. It gives two important meanings: (1) when the model residuals present a Gaussian distribution in the time domain, it indicates the GPS position time series have been well described by optimal model parameters. (2) Residuals can be used in common error removing, and the mean value represents the observation precision. The parameter  $\tau_j$  is given different values for various stations and earthquake events to make the best time series fit.

## 5.2 Noise Analysis

In the past most studies took GPS time series observation errors as a random process with time-independent white noise. The time-independent errors can be reduced or eliminated through taking average of a large amount of data. Johnson and Agnew (1995) studied California cGPS data and found that if the time-dependent noises are not removed, we may take the noise as a strain variation with time signal and give rise to incorrect geophysical interpretation. Without considering the time-dependent color noise the error will be underestimated and the parameter precision overestimated (e.g., velocity field). The uncertainty of velocity components taking into account the time-dependent color noise can be four times the white noise only. Furthermore, the estimated velocity filed may also be slightly changed (Langbein and Johnson 1997; Zhang et al. 1997; Mao et al. 1999). In the low-latitude region the error is significantly enlarged, especially on the vertical component. The error could be underestimated as large as 10 times. The atmosphere in the low-latitude area contains abundant water vapor, which seri-

ously affects GPS signal transmission. The water vapor is correlated with the seasons. The GPS position time series in Taiwan is usually more scattered during the summer. Therefore, we should consider the noise characteristics in the GPS position time series to be time-dependent.

GPS time series noise is a power-law process, its power-spectrum,  $P_x(f)$ , can be expressed as the following equation:

$$P_x(f) = P_0 \left( \frac{f}{f_0} \right)^k \quad (2)$$

Where  $f$  is temporal frequency,  $P_0, f_0$  are normalizing constant and  $k$  is spectral index. The spectral index  $k$  is used to define three kinds of color noise which is white noise ( $k = 0$ ), flicker noise ( $k = -1$ ), and random-walk noise (Brownian motion,  $k = -2$ ). Noise can be a combination of different noise modes, i.e., white-noise-only model (WH), white noise + flicker noise model (FN), or white noise + random-walk noise model (RW). By stacking the power spectral densities from time series analysis residuals, we are able to estimate the spectral index to distinguish the noise characteristics (Tsai 2004, 2013; Tsai et al. 2007). Stacking the 281 Taiwan cGPS stations used in this paper, the spectra indexes for the east, north, and vertical components are -0.72, -0.77, and -0.57, respectively (Fig. 13). This result indicates the Taiwan cGPS data noise model should be white noise + flicker noise model (FN), consistent with the results from previous studies that  $k$  of GPS time series is usually between 0 and -1 (Zhang et al. 1997; Mao et al. 1999; Nikolaidis 2002; Yu et al. 2003). A more realistic noise model can give a better estimate of the full covariance matrix and model parameters in GPS position time series. We used the Maximum-likelihood Method (MLE) to estimate the correlated noise amplitude (Williams 2003). The best-fit noise model (FN model) to the data is

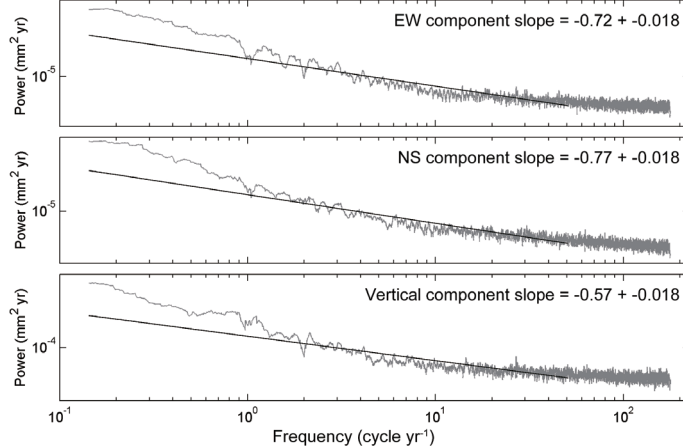


Fig. 13. Stacking the power spectral density of 281 cGPS sites. The slopes of -0.72, -0.77, and -0.57 indicate the spectral index for the east, north and up components, respectively.

that which maximizes the probability function with the covariance matrix used on re-weighting the time series model parameters to obtain more realistic parameter errors.

### 5.3 Common-Mode Error

The GPS position time series can be used to better understand the spatial and temporal variations in crustal deformation. Therefore, it is important to identify the signal characteristics in the GPS time series. Removing the systematic errors can effectively improve the data precision and identify signals in the time series. Common-mode error is a kind of systematic error coming from poor constraint in data processing. Wdowinski et al. (1997) pointed out the common errors of all sites are the average from the summation of all station errors and it can be removed by subtracting the GPS position times series data deviation in three components. Tabei and Amin (2002) also indicated the GPS time series errors approach the same value when the total number of stations for common-error-estimation reaches a certain quantity. In other words, removing common error will not affect the velocity field result, but improve the data precision instead. For example, the seasonal GPS position time series signal errors can be effectually reduced by removing the common error. The common error can be obtained by stacking the GPS position time series model residuals for some specified stations with good data quality, uniformly disturbed, and long time period. The common-mode error  $\epsilon_i$  can be represented as the following equations:

$$\epsilon_i = \begin{cases} 0 & : S_i(t_i) < 3 \\ \sum_{s=1}^{S_i} \frac{\gamma_{i,s}}{\sigma_{i,s}^2} & : S_i(t_i) \geq 3 \end{cases} \quad (3)$$

Where  $\gamma(t_i)$  and  $S_i(t_i)$  are the time series analysis model residuals and number of stations at a certain time,  $t_i$ . The common error is calculated only when the number of stations is greater than 3 at that day. Here  $i = 1, 2, 3, \dots, N$ , indicates from day one to day  $N$ .

We chose 50 relatively stable stations with longer time period to estimate the common-mode error in the Taiwan area. Figure 14 present the data span for 50 sites for common-mode error estimation, with nearly all sites having data periods longer than 6.5 years. By stacking these 50 fiducial sites the common-mode errors are 1.3, 1.2, and 2.7 mm in the east, north, and vertical components, respectively. Figure 15 shows the common-mode error distribution in the E, N, U components. To evaluate if any common-mode error directionality occurs in the Taiwan area, we calculated the average distribution slope in Fig. 15 using linear regression. The results show the slopes are almost zero in the E, N, U components, indicating no significant common-mode error directionality. The root-mean-square (RMS) value time series for the common-mode errors show larger values during the summer time (Fig. 16). After common-mode error corrections we re-modeled all parameters for the 281 cGPS position time series. The results indicate the GPS data precision was been further improved by removing the common-mode errors. The standard errors for the 281 cGPS stations decreased from 2.7, 2.4, and 7.7 to 2.3, 1.9, and 6.9 mm in the east, north and up components, respectively.

Figure 17 shows the position time series with FN model and common-mode error correction for the CHEN station (Chenkung, Taitung) in the ENU, respectively. The blue solid circles and light gray bars indicate the observed daily solutions and their formal error. The pink line indicates model predictions. The dashed line denotes the occurrence time for the 2008 Taitung earthquake (15 April 2008,  $M_L = 5.1$ ). The smoothing model predictions fit the observed GPS position time series very well. The GPS position time series figures

for the other 281 stations used in this study can be found at the GDMS website (<http://gdms.cwb.gov.tw/index.php>) of CWB. Figure 18 presents the CHEN model residuals in the ENU, respectively. The random model residuals distribution indicates the CHEN time series position is well corrected. The model results linear rates represent a more accurate velocity field. Tables 1 and 2 give the 2007 - 2013 ITRF2008 velocities and velocities relative to S01R (Paisha, Penghu) of cGPS sites. DASI and FKDO velocities are estimated using only data before 2011 to exclude the large scattering data due to bad sky visibility.

## 6. TAIWAN VELOCITY FIELD FROM 2007 - 2013

We derived a 2007 - 2013 velocity field based on the time series analysis results from 281 cGPS stations in the Taiwan area. Figures 19 - 21 show the ITRF2008 velocities and velocities with respect to S01R in the horizontal and vertical components, respectively. The error ellipse on the tip of each velocity vector indicates 95% confidence interval of uncertainty for the horizontal velocity (Figs. 19 and 21). On the other hand, the black cross represents various scales of rates and errors in vertical velocity. The red and blue color circles indicate uplift and subsidence, respectively (Fig. 20). It should be noted that stations with time periods less than 3 years and bad data quality are not shown.

The ITRF2008 horizontal velocity field in Fig. 19 is consistent with the plate motion direction which reveals the oblique collision between the Philippine Sea Plate and Eurasian Plate (Angelier 1986). The S01R station located at the Eurasia Plate are moving southeastward with a velocity of about 34 mm yr<sup>-1</sup>. From the west coast to the Western Foothills (WF), the velocities show ESE direction motion at a rate of about 21 - 33 mm yr<sup>-1</sup>. The velocity decreases eastward to 0 - 5 mm yr<sup>-1</sup> in the Central Range. The LANY station, located at the Philippine Sea Plate, is moving northwestward with a rate of about 50 mm yr<sup>-1</sup>. Velocities in the Coastal Range still reach 40 mm yr<sup>-1</sup> in the NW direction. The significant velocity change is detected across the Longitude Valley Fault (LVF) which is the suture zone of two plates. Across the LVF there is about 20 - 30 mm yr<sup>-1</sup> velocity change. The velocities in northern and northeastern Taiwan are about 40 - 60 mm yr<sup>-1</sup> and reveal significant clockwise rotation. The velocity reaches a maximum value of about 60 mm yr<sup>-1</sup> at SUAO (Suauo, Ilan). A dramatic change in velocities is found in the region between Hualien and Ilan, which is the place that the Philippine Sea Plate starts to subduct underneath the Eurasian Plate. In southern Taiwan the velocity field between the Chishan Fault (CSF) and Chaozhou Fault (CZF) shows obvious tectonic extrusion, moving in WSW-SSW directions with a rate of about 23 - 44 mm yr<sup>-1</sup>.

The ITRF2008 vertical velocity field in Fig. 20 indicates uplift sites are found mostly in the hill and mountain areas of the WF and Central Range. The Jiuchiunkeng-Muchiliao-Li-

uchia Fault system (JMLF) seems to be a vertical velocities change boundary. There are about 3 - 10 mm yr<sup>-1</sup> uplift and 5 - 14 mm yr<sup>-1</sup> subsidence rates in the eastern and western

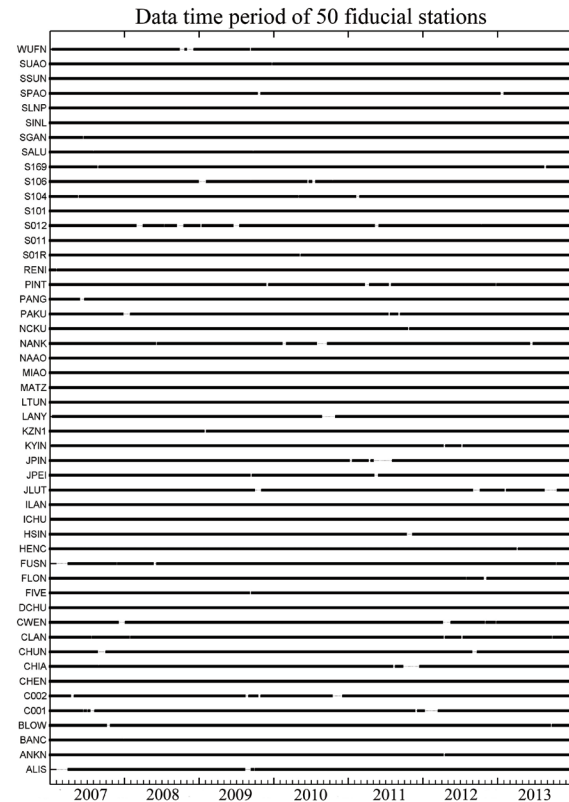


Fig. 14. The data time period of 50 fiducial stations used for stacking common-mode errors. The black dots indicate data are available for the cGPS sites at that time.

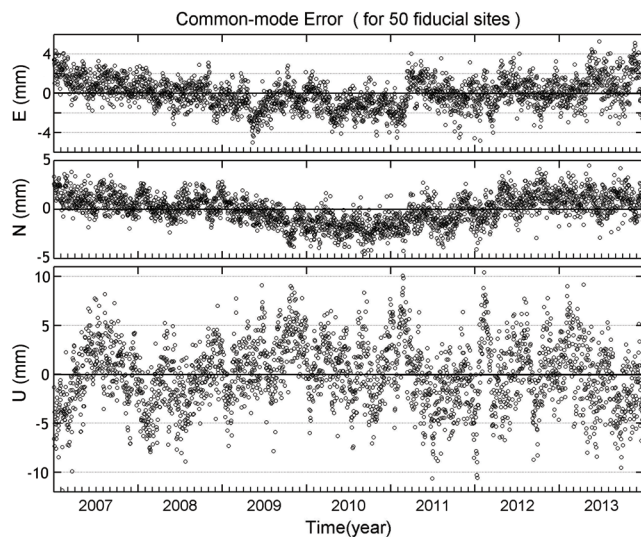


Fig. 15. The common-mode error distribution in the east, north and up components, respectively. The black circle indicates common-mode error from stacking 50 fiducial sites in Fig. 14. The slopes of the straight lines are all near zero in the E, N, and U components.

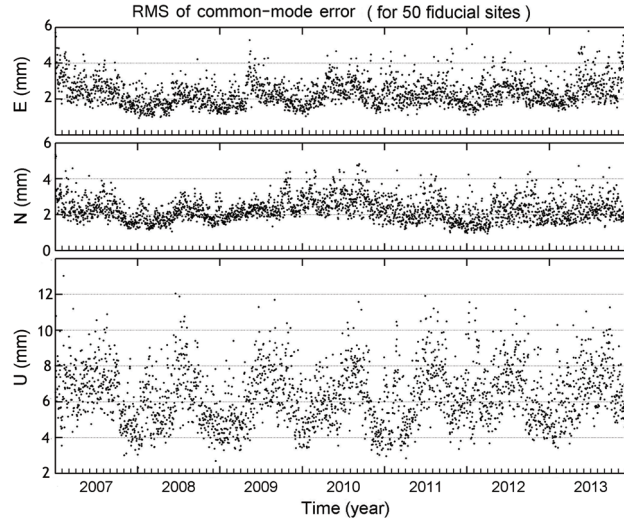


Fig. 16. RMS distribution of common-mode errors in the east, north and up components, respectively.

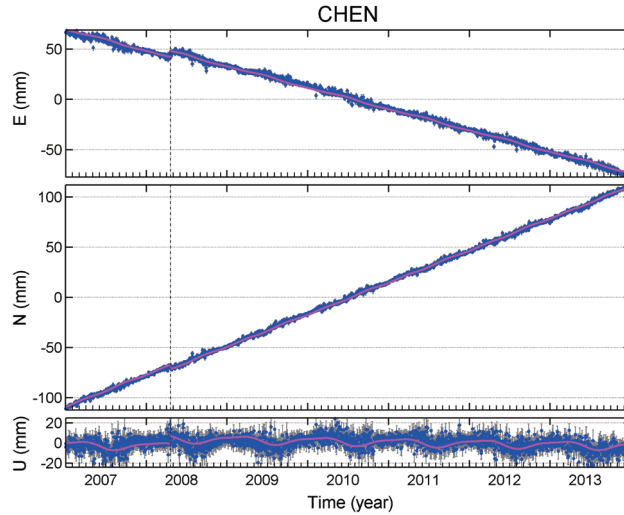


Fig. 17. CHEN station position time series analysis results in the east, north and up components, respectively. The blue solid circles and light gray bars indicate the observed daily solutions and their formal errors; the pink line indicates model predictions. The dashed line denotes the occurrence time of 2008 Taitung earthquake ( $M_L = 5.1$ ).

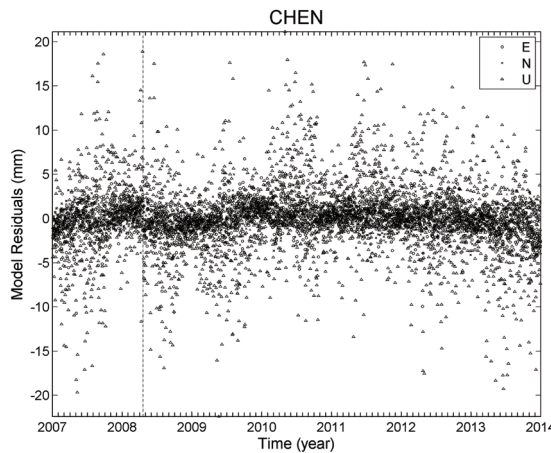


Fig. 18. Model residuals for the CHEN station in the east, north and up components, respectively.

Table 1. ITRF2008 velocities of cGPS stations in the Taiwan area (2007 - 2013).

Site	Lon. (°)	Lat. (°)	$V_e$ (mm yr $^{-1}$ )	$V_n$ (mm yr $^{-1}$ )	$V_u$ (mm yr $^{-1}$ )	Period (year)
8118	120.55298	23.46298	16.4 ± 0.4	-7.7 ± 0.5	1.0 ± 3.0	2007.0 - 2014.0
AKND	120.35726	22.80331	-8.0 ± 1.0	-21.6 ± 0.3	3.2 ± 1.4	2007.0 - 2014.0
ALIS	120.81329	23.50817	2.9 ± 0.3	-6.1 ± 0.4	1.0 ± 1.6	2007.3 - 2014.0
ANKN	121.52472	24.95910	33.6 ± 0.3	-8.8 ± 0.3	-1.8 ± 1.5	2007.0 - 2014.0
BALN	121.42612	24.69948	28.6 ± 0.4	-3.0 ± 0.3	-1.0 ± 1.8	2007.0 - 2014.0
BANC	121.44210	24.99765	33.1 ± 0.3	-9.0 ± 0.4	-1.1 ± 1.8	2007.0 - 2014.0
BANP	120.30540	22.69313	-17.4 ± 1.1	-37.0 ± 1.3	2.6 ± 6.2	2007.3 - 2013.2
BLOW	121.57124	24.17175	22.8 ± 0.5	-6.1 ± 0.5	1.8 ± 2.9	2007.0 - 2014.0
C001	120.61239	23.41794	7.1 ± 0.3	-4.5 ± 0.5	2.5 ± 2.0	2007.0 - 2014.0
C002	120.57719	23.36174	6.2 ± 0.3	-5.5 ± 0.4	4.4 ± 1.8	2007.0 - 2014.0
CHEN	121.37358	23.09740	-21.5 ± 0.3	31.6 ± 0.2	-1.1 ± 1.6	2007.0 - 2014.0
CHIA	120.43320	23.49597	22.8 ± 0.2	-8.6 ± 0.3	-1.8 ± 1.4	2007.0 - 2014.0
CHIH	121.20598	23.11584	-2.9 ± 0.9	6.1 ± 0.3	-4.0 ± 3.0	2007.0 - 2014.0
CHIN	120.58215	24.27101	31.2 ± 0.7	-12.5 ± 1.0	4.0 ± 5.0	2007.0 - 2014.0
CHIU	120.82890	23.94538	13.7 ± 0.6	-0.1 ± 0.3	2.4 ± 1.9	2007.1 - 2014.0
CHKU	120.09275	23.05584	29.3 ± 0.2	-12.7 ± 0.2	-3.5 ± 1.1	2007.0 - 2014.0
CHNL	120.56347	23.37714	13.2 ± 3.4	-1.0 ± 3.3	-5.0 ± 16.6	2007.8 - 2009.6
CHNT	121.66189	24.14921	21.0 ± 0.5	-8.9 ± 0.6	-1.9 ± 3.1	2007.0 - 2014.0
CHUA	120.55730	24.06605	29.9 ± 0.3	-10.8 ± 0.4	-5.7 ± 2.6	2007.0 - 2014.0
CHUK	120.60472	23.43871	14.6 ± 1.1	-7.3 ± 1.0	6.3 ± 6.7	2011.0 - 2014.0
CHUL	121.12568	23.13236	-0.9 ± 0.7	2.6 ± 0.4	3.4 ± 2.5	2007.0 - 2014.0
CHUN	121.39310	23.45285	-13.7 ± 0.5	28.0 ± 0.4	-5.5 ± 1.7	2007.0 - 2014.0
CHYN	120.29080	23.39327	26.8 ± 0.4	-10.9 ± 0.2	-5.8 ± 1.8	2007.0 - 2014.0
CLAN	121.51200	24.60225	34.9 ± 0.3	-6.2 ± 0.3	3.4 ± 2.0	2007.0 - 2014.0
CLON	120.57960	22.43005	-24.5 ± 0.3	-12.2 ± 0.3	-15.8 ± 3.2	2007.0 - 2014.0
CTOU	120.27784	22.75468	-7.6 ± 0.4	-24.4 ± 0.4	-3.1 ± 2.0	2007.0 - 2014.0
CWEN	120.45276	23.47304	21.6 ± 0.3	-7.3 ± 0.3	-1.3 ± 1.3	2007.0 - 2014.0
DAHU	120.87183	24.42288	26.7 ± 0.4	-9.3 ± 0.5	-2.3 ± 1.5	2007.0 - 2014.0
DAJN	120.86497	22.31130	-11.2 ± 0.4	2.1 ± 0.3	1.0 ± 1.7	2007.0 - 2014.0
DANL	120.75191	22.20413	-15.9 ± 1.1	-4.3 ± 1.1	0.4 ± 5.9	2010.2 - 2014.0
DASI	120.94441	22.47842	-4.6 ± 3.4	-0.2 ± 2.0	18.7 ± 10.2	2007.0 - 2011.0
DCHU	121.28057	23.21318	-13.0 ± 0.4	27.3 ± 0.3	3.9 ± 2.1	2007.0 - 2014.0
DNFU	121.48228	23.68512	-5.5 ± 0.9	15.3 ± 0.7	-6.9 ± 2.8	2007.0 - 2014.0
DONA	120.70351	22.91562	-23.1 ± 0.4	-10.4 ± 0.3	7.4 ± 1.7	2007.0 - 2014.0
DPIN	120.93280	24.04308	11.6 ± 0.3	-1.4 ± 0.2	2.0 ± 1.7	2007.0 - 2014.0
DSIN	121.39803	23.63121	2.2 ± 0.7	8.8 ± 0.4	-7.6 ± 3.0	2007.0 - 2014.0
DULI	121.33059	23.02566	-16.7 ± 1.1	32.0 ± 0.7	8.6 ± 4.0	2007.0 - 2014.0
ERLN	120.41955	23.79759	31.4 ± 0.8	-10.4 ± 0.4	-11.3 ± 3.3	2007.0 - 2014.0
ERPN	121.16611	22.94217	-21.9 ± 0.3	27.5 ± 0.3	5.7 ± 2.0	2007.0 - 2014.0
FENP	121.51942	23.59845	-16.1 ± 0.7	32.9 ± 0.5	-4.3 ± 2.9	2007.0 - 2014.0
FIVE	121.78107	25.07105	35.5 ± 0.3	-10.9 ± 0.4	-1.2 ± 1.2	2007.0 - 2014.0
FKDO	120.85627	23.68355	6.7 ± 2.5	1.7 ± 1.3	-8.0 ± 12.0	2007.0 - 2011.0
FLON	121.93748	25.02037	35.7 ± 0.4	-13.1 ± 0.7	-2.9 ± 2.0	2007.0 - 2014.0
FNGU	120.72445	24.03516	21.6 ± 0.3	-6.9 ± 0.2	-2.0 ± 1.2	2007.0 - 2014.0
FUNY	120.32017	23.92231	32.5 ± 0.3	-10.9 ± 0.2	-12.7 ± 2.9	2007.0 - 2014.0
FUQE	120.82331	24.01115	18.2 ± 0.5	-2.9 ± 0.3	-0.8 ± 2.1	2008.4 - 2014.0
FUSN	121.33146	24.79904	31.6 ± 0.4	-5.8 ± 0.4	0.8 ± 2.1	2007.3 - 2014.0
GAIS	120.59062	23.08029	-9.1 ± 0.4	-8.2 ± 0.3	9.0 ± 1.8	2007.0 - 2014.0
GS01	121.50816	24.98200	34.3 ± 0.4	-7.4 ± 0.4	1.2 ± 1.7	2007.0 - 2014.0
GS02	120.98234	24.80972	29.3 ± 0.4	-10.0 ± 0.3	-3.4 ± 1.5	2007.0 - 2014.0

Note: Lon. and Lat. are the longitude and latitude of GPS sites;  $V_e$ ,  $V_n$ , and  $V_u$  are the ENU of ITRF2008 station velocities with standard errors, respectively; period shows the start and end time of observation period.

Table 1. (Continued)

Site	Lon. (°)	Lat. (°)	$V_e$ (mm yr <sup>-1</sup> )	$V_n$ (mm yr <sup>-1</sup> )	$V_u$ (mm yr <sup>-1</sup> )	Period (year)
GS03	121.04407	24.77660	30.0 ± 0.6	-7.9 ± 0.6	-1.1 ± 1.4	2007.0 - 2014.0
GS04	120.50679	23.59152	25.6 ± 1.0	-8.9 ± 0.8	-0.8 ± 5.2	2007.0 - 2009.9
GS05	120.56840	23.56711	18.4 ± 0.3	-7.1 ± 0.2	0.4 ± 1.4	2007.0 - 2014.0
GS06	120.55422	23.46561	16.3 ± 0.3	-8.4 ± 0.3	1.3 ± 1.4	2007.0 - 2014.0
GS07	120.65483	23.48291	12.4 ± 0.3	-6.5 ± 0.3	4.1 ± 1.6	2007.0 - 2014.0
GS08	121.50149	25.20373	32.6 ± 0.5	-9.3 ± 0.6	-1.2 ± 2.0	2007.0 - 2014.0
GS09	121.65193	25.20861	34.7 ± 0.3	-10.5 ± 0.3	0.2 ± 1.6	2007.0 - 2014.0
GS10	121.46155	25.14615	30.0 ± 0.5	-10.4 ± 0.4	-5.3 ± 1.9	2007.0 - 2014.0
GS11	121.49877	25.13357	31.4 ± 0.4	-9.3 ± 0.3	-3.2 ± 1.8	2007.0 - 2014.0
GS12	121.38276	25.05303	32.8 ± 0.4	-8.6 ± 0.3	1.1 ± 1.7	2007.0 - 2014.0
GS13	121.45224	25.02001	33.6 ± 0.6	-8.8 ± 0.4	-5.8 ± 3.2	2007.0 - 2014.0
GS14	120.95945	24.80322	31.0 ± 0.2	-9.0 ± 0.2	-1.4 ± 1.2	2007.0 - 2014.0
GS15	120.99050	24.76665	30.3 ± 0.2	-8.3 ± 0.2	-0.2 ± 1.2	2007.0 - 2014.0
GS16	121.04161	24.74787	29.9 ± 0.3	-7.6 ± 0.2	0.1 ± 1.3	2007.0 - 2014.0
GS17	120.60584	23.56115	14.6 ± 0.3	-6.2 ± 0.3	2.4 ± 1.5	2007.0 - 2014.0
GS18	120.47378	23.48498	21.1 ± 0.3	-8.7 ± 0.3	-0.5 ± 1.2	2007.0 - 2014.0
GS19	121.67981	25.07174	35.9 ± 0.4	-10.6 ± 0.5	-0.1 ± 2.2	2007.0 - 2012.4
GS20	121.94321	24.84190	44.5 ± 0.4	-19.9 ± 0.6	-18.8 ± 1.7	2007.0 - 2014.0
GS21	120.51241	24.09648	30.1 ± 0.2	-11.3 ± 0.2	-2.6 ± 1.3	2007.0 - 2014.0
GS22	120.60390	24.09133	28.5 ± 0.2	-10.3 ± 0.2	-3.1 ± 1.3	2007.0 - 2014.0
GS23	120.64816	24.09370	27.9 ± 0.3	-9.6 ± 0.2	-1.6 ± 1.8	2007.0 - 2014.0
GS24	120.52644	24.02564	29.8 ± 0.3	-11.1 ± 0.2	-7.6 ± 2.1	2007.0 - 2014.0
GS25	120.64059	23.98667	27.5 ± 0.3	-9.6 ± 0.3	-3.4 ± 1.9	2007.0 - 2014.0
GS26	120.57870	23.82489	27.1 ± 0.3	-9.9 ± 0.2	-1.4 ± 1.6	2007.0 - 2014.0
GS27	120.64631	23.87021	27.9 ± 0.3	-9.9 ± 0.2	-1.7 ± 1.8	2007.0 - 2014.0
GS28	120.21358	23.07986	26.1 ± 0.5	-11.9 ± 0.3	-3.3 ± 2.9	2007.0 - 2014.0
GS29	120.31755	23.07537	21.4 ± 0.4	-12.7 ± 0.3	3.2 ± 1.3	2007.0 - 2014.0
GS30	120.22612	23.02032	20.1 ± 0.3	-11.9 ± 0.3	0.7 ± 1.3	2007.0 - 2014.0
GS31	120.27588	23.01875	15.7 ± 0.5	-13.2 ± 0.2	-2.0 ± 1.3	2007.0 - 2014.0
GS32	120.33584	23.02714	12.0 ± 0.5	-15.7 ± 0.3	1.7 ± 1.3	2007.0 - 2014.0
GS33	120.18695	22.96369	20.8 ± 0.3	-12.1 ± 0.2	-2.5 ± 1.2	2007.0 - 2014.0
GS34	120.27632	22.93612	8.5 ± 0.6	-13.1 ± 0.2	3.6 ± 1.3	2007.0 - 2014.0
GS35	120.30849	22.93581	8.0 ± 0.5	-14.2 ± 0.2	4.6 ± 1.6	2007.0 - 2014.0
GS36	120.62530	24.36200	29.8 ± 0.3	-10.6 ± 0.2	-1.8 ± 1.2	2007.0 - 2014.0
GS37	120.71540	24.32860	27.6 ± 0.3	-9.8 ± 0.3	-2.4 ± 1.3	2007.0 - 2014.0
GS38	120.60060	24.27980	30.0 ± 0.3	-11.3 ± 0.2	-2.7 ± 1.3	2007.0 - 2014.0
GS39	120.52960	24.18440	30.3 ± 0.3	-11.0 ± 0.2	-2.4 ± 1.2	2007.0 - 2014.0
GS40	120.57630	24.18120	29.8 ± 0.2	-10.1 ± 0.3	-2.4 ± 1.1	2007.0 - 2014.0
GS41	120.44490	23.37760	21.2 ± 0.4	-8.5 ± 0.5	-3.8 ± 2.1	2007.9 - 2014.0
GS42	120.45200	23.27320	13.3 ± 0.4	-9.1 ± 0.3	5.0 ± 1.7	2007.9 - 2014.0
GS43	120.37360	23.25720	23.2 ± 0.4	-10.0 ± 0.3	-1.2 ± 1.7	2007.9 - 2014.0
GS44	120.40040	23.22220	16.2 ± 0.3	-11.1 ± 0.3	6.3 ± 1.7	2007.9 - 2014.0
GS45	120.72800	22.75250	-25.7 ± 0.7	-9.2 ± 0.6	9.0 ± 4.2	2009.0 - 2014.0
GS46	120.63950	22.52970	-25.6 ± 0.6	-10.5 ± 0.6	3.1 ± 4.4	2009.0 - 2014.0
GS47	120.73700	21.95060	-5.9 ± 2.2	-6.1 ± 1.0	-30.1 ± 5.0	2009.0 - 2013.6
GS51	120.54006	23.00022	-16.1 ± 0.7	-14.7 ± 0.6	6.5 ± 3.3	2010.0 - 2014.0
GS52	120.65472	23.03402	-18.6 ± 0.7	-11.2 ± 0.6	6.5 ± 3.5	2010.0 - 2014.0
GS53	120.39831	22.83998	-10.0 ± 0.7	-19.5 ± 0.6	8.5 ± 4.1	2010.0 - 2014.0
GS54	120.45209	22.83710	-22.1 ± 0.9	-16.4 ± 0.7	0.4 ± 4.0	2010.0 - 2013.5
GS55	120.60224	22.85069	-24.6 ± 0.8	-11.2 ± 0.8	2.7 ± 3.5	2009.9 - 2014.0
GS56	120.60173	22.70388	-25.8 ± 0.8	-12.6 ± 0.6	1.5 ± 4.0	2010.0 - 2014.0
GS57	120.76485	22.12753	-14.9 ± 1.4	-3.8 ± 0.8	1.8 ± 4.8	2010.0 - 2014.0

Table 1. (Continued)

Site	Lon. (°)	Lat. (°)	$V_e$ (mm yr <sup>-1</sup> )	$V_n$ (mm yr <sup>-1</sup> )	$V_u$ (mm yr <sup>-1</sup> )	Period (year)
GS58	120.83892	22.12637	-9.3 ± 1.0	2.3 ± 0.7	-2.1 ± 5.0	2010.0 - 2014.0
GS59	120.70439	22.05740	-17.8 ± 0.9	-12.3 ± 0.7	-2.9 ± 4.2	2010.0 - 2014.0
GS60	120.80973	22.00754	-9.9 ± 1.3	1.2 ± 0.9	1.6 ± 5.2	2010.0 - 2014.0
GS61	121.20048	24.67880	28.9 ± 1.2	-4.1 ± 0.8	1.0 ± 6.5	2010.8 - 2014.0
GS62	121.24302	24.73348	30.5 ± 1.1	-4.2 ± 0.7	0.8 ± 5.1	2010.8 - 2014.0
GS63	120.62683	23.54326	13.9 ± 1.1	-6.9 ± 1.9	4.7 ± 4.4	2010.7 - 2014.0
GS64	120.71215	23.40764	1.8 ± 0.9	-7.1 ± 0.8	4.5 ± 4.7	2010.7 - 2014.0
GS66	120.74150	23.45619	3.0 ± 0.9	-7.2 ± 0.9	6.7 ± 4.5	2010.7 - 2014.0
GS67	120.67515	23.33968	1.7 ± 0.9	-5.7 ± 0.7	4.5 ± 4.3	2010.7 - 2014.0
GS68	120.48770	23.60710	23.9 ± 1.2	-10.5 ± 0.7	-4.8 ± 6.3	2011.0 - 2014.0
GS69	121.37797	24.96777	34.2 ± 1.9	-9.7 ± 1.5	1.5 ± 11.4	2011.7 - 2014.0
GUKN	120.58878	23.64586	24.0 ± 0.4	-6.7 ± 0.2	-0.6 ± 2.0	2007.0 - 2014.0
GUKW	121.00655	24.20220	16.6 ± 0.5	-0.1 ± 0.4	2.8 ± 3.8	2007.0 - 2014.0
HANS	121.68714	24.60951	51.1 ± 0.4	-13.3 ± 0.7	-1.4 ± 2.1	2007.0 - 2014.0
HENC	120.74645	22.00393	-20.2 ± 0.7	-10.5 ± 0.4	-5.1 ± 2.2	2007.0 - 2014.0
HERI	121.58092	25.29444	32.9 ± 0.4	-10.2 ± 0.3	-0.1 ± 1.6	2007.0 - 2014.0
HLIU	120.99417	23.79303	-0.5 ± 0.7	2.6 ± 0.7	1.6 ± 3.3	2007.0 - 2014.0
HOKN	120.13488	23.18838	29.6 ± 0.2	-12.2 ± 0.2	-7.0 ± 1.3	2007.0 - 2014.0
HOPN	120.89488	24.17078	16.2 ± 0.5	-4.1 ± 0.8	-9.2 ± 3.3	2007.0 - 2014.0
HRGN	121.40510	23.55528	-8.0 ± 0.5	18.6 ± 0.4	-12.2 ± 2.4	2007.0 - 2014.0
HSIN	121.01425	24.82775	30.9 ± 0.3	-9.6 ± 0.2	-1.1 ± 1.3	2007.0 - 2014.0
HSUE	121.02645	24.28059	15.5 ± 0.7	0.0 ± 0.5	-3.3 ± 2.6	2007.0 - 2014.0
HUAL	121.61351	23.97538	8.3 ± 0.6	3.0 ± 0.4	-6.5 ± 2.1	2007.0 - 2014.0
HUAN	121.27262	24.14347	14.7 ± 0.7	4.1 ± 0.8	1.1 ± 1.8	2007.1 - 2014.0
HUAP	121.74944	24.30900	36.1 ± 0.7	-23.3 ± 0.6	-2.5 ± 3.2	2007.0 - 2014.0
HUWE	120.28662	23.72940	30.8 ± 0.2	-10.0 ± 0.2	-29.7 ± 2.7	2007.0 - 2014.0
HUYA	121.02941	24.09233	8.7 ± 0.4	-0.8 ± 0.3	6.5 ± 1.6	2007.0 - 2014.0
ICHU	120.27930	23.36066	26.5 ± 0.3	-10.7 ± 0.3	-10.0 ± 1.5	2007.0 - 2014.0
ILAN	121.75662	24.76404	39.3 ± 0.3	-16.0 ± 0.3	-7.9 ± 1.7	2007.0 - 2014.0
JLUT	120.62278	22.32996	-22.2 ± 0.4	-10.4 ± 0.4	0.4 ± 1.9	2007.0 - 2014.0
JONP	120.52400	23.42297	17.8 ± 0.3	-7.2 ± 0.3	2.7 ± 1.3	2007.0 - 2014.0
JPEI	121.37139	23.53160	3.6 ± 0.7	10.7 ± 0.5	-4.0 ± 2.6	2007.0 - 2014.0
JPIN	121.35889	23.34108	-10.8 ± 0.4	32.1 ± 0.3	7.0 ± 1.8	2007.0 - 2014.0
JSUI	121.42389	23.49198	-12.7 ± 0.6	29.3 ± 0.3	-0.2 ± 2.7	2007.0 - 2014.0
JYAN	121.22634	24.24247	22.3 ± 0.5	5.9 ± 0.5	3.8 ± 1.8	2007.0 - 2014.0
KASU	120.63298	22.81019	-26.5 ± 0.8	-13.3 ± 0.8	4.2 ± 2.6	2007.3 - 2014.0
KNKO	121.50574	23.47221	-17.0 ± 0.3	35.2 ± 0.3	-5.9 ± 2.0	2007.0 - 2014.0
KSHI	121.17603	24.77666	29.3 ± 0.9	-7.1 ± 0.5	-4.4 ± 8.2	2007.0 - 2014.0
KUAN	121.16425	23.04968	0.9 ± 0.7	3.0 ± 0.6	-5.5 ± 3.1	2007.0 - 2014.0
KULN	120.50702	23.33098	8.4 ± 0.4	-7.9 ± 0.3	7.0 ± 1.5	2007.0 - 2014.0
KYIN	121.08042	25.04105	30.9 ± 0.3	-10.0 ± 0.2	1.4 ± 1.3	2007.0 - 2014.0
KZN1	120.69798	23.94625	25.1 ± 0.3	-9.2 ± 0.2	-4.3 ± 1.6	2007.0 - 2014.0
LAIG	120.73990	23.52940	4.9 ± 0.5	-6.9 ± 0.5	4.7 ± 2.6	2008.6 - 2014.0
LANY	121.55810	22.03731	-37.5 ± 0.6	33.7 ± 0.8	1.6 ± 1.9	2007.0 - 2014.0
LAOL	120.68729	22.41192	-22.5 ± 1.3	-10.4 ± 0.8	2.2 ± 4.9	2007.0 - 2012.0
LGUE	120.63538	22.99290	-19.0 ± 0.7	-12.3 ± 0.4	9.8 ± 3.1	2007.0 - 2014.0
LIKU	120.52790	22.75861	-26.7 ± 0.7	-17.6 ± 0.6	4.6 ± 4.3	2007.0 - 2014.0
LIUC	120.36907	22.34667	-20.8 ± 1.1	-38.2 ± 0.6	-1.2 ± 4.3	2007.0 - 2013.9
LIYU	120.78180	24.34306	29.7 ± 0.7	-12.2 ± 0.5	8.2 ± 3.2	2007.0 - 2014.0
LNCH	120.40261	22.99458	7.8 ± 0.5	-18.6 ± 0.2	12.6 ± 1.3	2007.0 - 2014.0
LNKO	121.37818	25.07637	32.9 ± 0.4	-8.5 ± 0.2	0.0 ± 2.3	2007.0 - 2014.0
LONT	121.13056	22.90631	-7.7 ± 0.4	8.9 ± 0.9	4.1 ± 2.1	2007.0 - 2014.0

Table 1. (Continued)

Site	Lon. (°)	Lat. (°)	$V_e$ (mm yr <sup>-1</sup> )	$V_n$ (mm yr <sup>-1</sup> )	$V_u$ (mm yr <sup>-1</sup> )	Period (year)
LOYE	120.70120	23.46860	7.6 ± 0.5	-6.2 ± 0.5	1.4 ± 2.2	2008.6 - 2014.0
LSAN	121.18216	24.02934	8.7 ± 0.5	-0.1 ± 0.4	6.9 ± 1.7	2007.0 - 2014.0
LTUN	121.77162	24.70003	44.1 ± 0.4	-18.3 ± 0.3	-6.6 ± 2.1	2007.0 - 2014.0
LUGU	120.74769	23.75226	12.9 ± 0.9	-3.3 ± 0.8	2.5 ± 6.4	2007.0 - 2010.2
LUKN	120.43513	24.06001	29.5 ± 0.3	-11.3 ± 0.2	-6.1 ± 1.9	2007.0 - 2014.0
LUSN	121.18605	24.03519	7.7 ± 1.0	-1.6 ± 0.6	1.4 ± 3.4	2007.1 - 2014.0
MATZ	119.92306	26.16939	30.6 ± 0.3	-12.5 ± 0.2	-0.5 ± 1.1	2007.0 - 2014.0
MESN	120.82626	23.26363	-1.8 ± 0.5	-8.0 ± 0.3	8.3 ± 2.2	2007.0 - 2014.0
MFEN	121.17247	24.08216	3.3 ± 0.5	4.6 ± 0.3	4.3 ± 1.3	2007.0 - 2014.0
MIAO	120.81026	24.58345	27.8 ± 0.4	-9.5 ± 0.3	-0.7 ± 1.7	2007.0 - 2014.0
MINS	120.72090	23.27540	-0.7 ± 0.6	-5.7 ± 0.6	6.2 ± 2.6	2007.0 - 2012.0
MITO	120.26315	22.79585	6.8 ± 1.2	-18.6 ± 1.0	-0.3 ± 5.5	2007.0 - 2012.5
MLO1	120.55400	22.90000	-19.3 ± 0.7	-15.7 ± 0.4	-1.7 ± 3.0	2007.0 - 2012.0
MOTN	121.02685	23.20054	-1.0 ± 0.7	-5.3 ± 0.4	3.6 ± 2.4	2007.0 - 2014.0
NAAO	121.81021	24.44934	40.3 ± 0.5	-28.7 ± 0.6	-8.5 ± 1.8	2007.0 - 2014.0
NANK	120.27439	23.10199	25.6 ± 0.3	-12.5 ± 0.2	-1.6 ± 1.5	2007.0 - 2014.0
NCKU	120.27581	22.93845	8.0 ± 0.5	-12.9 ± 0.2	3.2 ± 1.5	2007.0 - 2014.0
NDHU	121.55081	23.89724	3.4 ± 0.5	6.3 ± 0.6	-5.6 ± 1.9	2007.0 - 2014.0
NEMN	120.42008	22.90812	-6.5 ± 0.4	-16.8 ± 0.3	8.3 ± 1.9	2007.0 - 2014.0
NHSI	121.45301	23.40621	-13.6 ± 0.6	34.4 ± 0.4	-2.5 ± 2.7	2007.0 - 2014.0
NIUT	121.56158	24.63478	37.4 ± 0.6	-6.0 ± 0.6	3.7 ± 4.0	2007.0 - 2014.0
NJOU	120.57141	22.50389	-25.7 ± 0.4	-12.8 ± 0.4	-11.3 ± 2.6	2007.0 - 2014.0
NSAN	121.38280	24.42820	27.9 ± 0.7	-1.2 ± 0.5	7.6 ± 2.9	2007.0 - 2014.0
NSHE	120.80090	24.22579	21.0 ± 0.3	-7.2 ± 0.3	1.3 ± 1.6	2007.0 - 2014.0
PAKU	120.63603	23.91568	27.0 ± 0.4	-10.2 ± 0.2	-1.8 ± 1.7	2007.0 - 2014.0
PANG	119.56374	23.56520	32.3 ± 0.2	-12.1 ± 0.2	-0.6 ± 1.5	2007.0 - 2014.0
PAOL	120.70287	23.10862	-12.9 ± 0.8	-9.2 ± 0.5	13.2 ± 1.7	2007.0 - 2014.0
PAOS	120.95028	24.71492	29.6 ± 0.5	-6.9 ± 0.4	1.4 ± 1.7	2007.0 - 2014.0
PEI1	120.16900	23.29400	26.0 ± 1.1	-13.7 ± 0.7	-13.5 ± 4.9	2007.0 - 2014.0
PEIN	121.12313	22.80107	-16.0 ± 0.5	-2.3 ± 0.4	2.3 ± 2.2	2007.2 - 2013.9
PENL	120.97604	24.53884	25.9 ± 1.7	-4.0 ± 1.2	-1.7 ± 7.1	2007.0 - 2014.0
PEPU	121.61034	24.01788	13.6 ± 0.6	-3.1 ± 0.8	-5.0 ± 2.6	2007.0 - 2014.0
PING	121.45434	23.31946	-16.9 ± 0.4	35.8 ± 0.3	-0.8 ± 1.9	2007.0 - 2014.0
PINT	120.64056	23.75606	27.8 ± 0.4	-9.3 ± 0.3	-3.5 ± 1.3	2007.0 - 2014.0
PLAN	121.08660	24.57895	30.4 ± 0.5	-3.0 ± 0.3	-0.9 ± 2.3	2007.0 - 2014.0
PLIN	121.71395	24.93362	32.9 ± 0.7	-10.9 ± 0.6	4.0 ± 3.2	2007.0 - 2014.0
PNCY	122.07944	25.62750	32.2 ± 0.6	-11.0 ± 0.4	-1.8 ± 3.1	2009.0 - 2013.4
PTUN	120.45968	22.64985	-25.2 ± 0.7	-21.7 ± 0.5	6.3 ± 3.7	2007.0 - 2014.0
PUSN	120.52011	23.96494	30.5 ± 1.7	-12.3 ± 1.4	-8.3 ± 6.1	2007.0 - 2014.0
RENI	120.50857	23.45894	18.7 ± 0.3	-8.4 ± 0.3	1.3 ± 1.3	2007.0 - 2014.0
S011	120.33945	23.20542	23.1 ± 0.5	-10.9 ± 0.6	0.5 ± 1.4	2007.0 - 2014.0
S012	120.48826	23.05947	-3.1 ± 0.4	-9.8 ± 0.3	5.3 ± 1.5	2007.0 - 2014.0
S016	120.80286	24.17955	19.0 ± 0.3	-8.5 ± 0.3	-0.8 ± 1.2	2007.0 - 2014.0
S01R	119.59237	23.65527	31.5 ± 0.2	-11.9 ± 0.2	0.5 ± 1.1	2007.0 - 2014.0
S101	121.61385	25.04045	33.9 ± 0.3	-9.9 ± 0.3	-1.6 ± 1.5	2007.0 - 2014.0
S102	121.55815	22.03721	-37.3 ± 1.5	36.9 ± 1.6	0.9 ± 5.7	2007.0 - 2010.8
S103	120.47519	23.56437	24.7 ± 0.3	-8.0 ± 0.2	-1.1 ± 1.3	2007.0 - 2014.0
S104	121.18938	22.82076	-22.6 ± 0.4	29.0 ± 0.3	2.0 ± 1.5	2007.0 - 2014.0
S105	121.11289	22.95165	0.5 ± 0.4	1.3 ± 0.3	-3.6 ± 1.6	2007.0 - 2014.0
S106	120.33409	23.05079	14.8 ± 0.3	-14.4 ± 0.5	2.9 ± 1.2	2007.0 - 2014.0
S167	120.93410	23.95442	10.7 ± 0.3	-1.1 ± 0.2	2.1 ± 1.4	2007.0 - 2014.0
S169	120.50331	22.94229	-15.0 ± 0.4	-12.4 ± 0.3	0.0 ± 1.6	2007.0 - 2014.0

Table 1. (Continued)

Site	Lon. (°)	Lat. (°)	$V_e$ (mm yr <sup>-1</sup> )	$V_n$ (mm yr <sup>-1</sup> )	$V_u$ (mm yr <sup>-1</sup> )	Period (year)
S170	120.76763	23.74596	8.9 ± 0.3	-2.3 ± 0.2	1.0 ± 1.4	2007.0 - 2014.0
S23R	120.60617	22.64498	-23.8 ± 0.4	-11.6 ± 0.3	1.9 ± 2.0	2007.0 - 2014.0
SALU	120.57830	24.14445	29.7 ± 0.3	-10.3 ± 0.2	-0.9 ± 1.5	2007.0 - 2014.0
SAND	120.64064	22.71727	-26.4 ± 0.4	-11.2 ± 0.4	4.1 ± 1.9	2007.0 - 2014.0
SANI	120.76873	24.41435	29.2 ± 0.5	-8.3 ± 0.4	-15.1 ± 7.4	2007.0 - 2014.0
SANJ	121.50087	25.26079	32.1 ± 0.3	-10.5 ± 0.3	-2.6 ± 1.9	2007.0 - 2014.0
SANL	120.76855	23.66448	8.2 ± 0.4	-0.6 ± 0.4	2.1 ± 1.4	2007.0 - 2014.0
SCHN	121.65159	24.12779	18.5 ± 0.8	-7.4 ± 0.6	-0.8 ± 3.7	2008.8 - 2014.0
SFON	121.01016	24.93289	31.1 ± 0.4	-10.9 ± 0.3	-3.7 ± 1.6	2007.0 - 2014.0
SGAN	120.34965	22.58127	-14.6 ± 0.4	-31.2 ± 0.4	-1.3 ± 1.7	2007.0 - 2014.0
SGUN	120.69188	24.27163	27.9 ± 0.3	-10.0 ± 0.2	-3.2 ± 1.4	2007.0 - 2014.0
SHAN	121.19949	23.10886	1.9 ± 0.5	6.5 ± 0.3	-7.2 ± 2.3	2007.0 - 2014.0
SHUL	121.56273	23.78761	2.8 ± 0.5	20.4 ± 0.4	-10.6 ± 2.1	2007.0 - 2014.0
SHWA	120.34781	23.02143	11.0 ± 0.5	-15.7 ± 0.2	3.6 ± 1.3	2007.0 - 2014.0
SILN	120.64604	23.16038	-3.6 ± 1.4	-9.3 ± 1.0	9.6 ± 7.0	2007.0 - 2009.6
SINL	121.25462	22.90829	-18.7 ± 0.5	30.2 ± 0.3	1.0 ± 1.8	2007.0 - 2014.0
SJPU	120.48126	23.42854	19.8 ± 0.3	-8.5 ± 0.3	-0.4 ± 2.0	2007.0 - 2014.0
SLIN	121.44140	23.81185	9.2 ± 0.7	3.6 ± 0.9	4.4 ± 3.9	2007.0 - 2014.0
SLNP	121.63563	24.75311	35.6 ± 0.3	-11.2 ± 0.3	-2.7 ± 1.4	2007.0 - 2014.0
SONA	120.98584	24.39781	23.8 ± 0.4	-4.2 ± 0.3	0.6 ± 1.7	2007.5 - 2014.0
SPA0	121.48486	24.20501	23.7 ± 0.6	-2.6 ± 0.4	10.2 ± 2.5	2007.0 - 2014.0
SSUN	120.37777	23.41415	22.8 ± 0.3	-9.7 ± 0.3	-1.6 ± 1.3	2007.0 - 2014.0
STA1	120.97926	24.63560	30.0 ± 0.5	-7.6 ± 0.5	3.1 ± 3.0	2008.1 - 2014.0
SUAB	121.86790	24.59391	51.4 ± 1.0	-37.1 ± 1.7	-4.4 ± 4.8	2007.0 - 2011.0
SUAN	120.29988	23.47757	27.7 ± 0.4	-11.0 ± 0.3	-6.0 ± 3.2	2007.0 - 2014.0
SUAO	121.86707	24.59239	51.4 ± 0.4	-36.4 ± 0.6	-4.6 ± 1.7	2007.0 - 2014.0
SUCH	120.90758	24.29107	24.8 ± 0.7	-10.2 ± 0.9	8.4 ± 4.1	2007.0 - 2014.0
SUN1	120.90835	23.88124	10.0 ± 0.3	-0.3 ± 0.2	2.4 ± 1.5	2007.0 - 2014.0
TAIP	121.67317	25.03452	34.9 ± 0.4	-10.6 ± 0.3	-2.7 ± 1.7	2007.2 - 2014.0
TANS	121.42689	25.18150	33.3 ± 1.9	-14.4 ± 1.2	4.5 ± 4.4	2007.0 - 2014.0
TAPE	121.23087	23.12557	-4.7 ± 0.5	8.1 ± 0.3	-10.8 ± 1.7	2007.0 - 2014.0
TAPO	121.23741	23.12706	-15.1 ± 0.6	29.3 ± 0.3	10.8 ± 2.0	2007.0 - 2014.0
TAPU	120.58541	23.25080	1.3 ± 0.4	-4.9 ± 0.4	5.4 ± 1.7	2007.0 - 2014.0
TATA	120.88705	23.48140	-10.9 ± 0.6	2.4 ± 0.5	2.8 ± 2.5	2007.0 - 2014.0
TEGS	120.65498	24.35621	29.6 ± 0.2	-10.4 ± 0.2	0.4 ± 1.3	2007.0 - 2014.0
TENC	120.91567	23.27779	9.7 ± 2.0	-5.7 ± 0.7	-1.3 ± 3.5	2007.0 - 2014.0
THAI	121.29559	24.60712	30.4 ± 0.5	-2.9 ± 0.3	2.8 ± 1.5	2007.0 - 2014.0
TMAL	120.95987	22.64892	-2.5 ± 0.7	-0.5 ± 0.6	0.7 ± 2.1	2007.0 - 2013.9
TOFN	120.92480	24.66204	29.3 ± 0.3	-8.5 ± 0.2	0.4 ± 1.4	2007.0 - 2014.0
TSHI	121.63276	25.25691	33.3 ± 0.4	-10.1 ± 0.3	-1.2 ± 2.0	2007.0 - 2014.0
TSIO	120.70410	24.47279	29.7 ± 0.3	-10.1 ± 0.2	0.7 ± 1.4	2007.0 - 2014.0
TSLN	120.71938	23.63432	11.6 ± 0.4	-4.7 ± 0.5	5.3 ± 2.1	2007.3 - 2012.8
TTSH	121.14762	22.74713	-12.6 ± 0.5	1.4 ± 0.4	-5.7 ± 2.9	2008.4 - 2014.0
TTUN	121.08070	22.76455	-10.8 ± 0.4	0.5 ± 0.5	-4.1 ± 1.8	2007.0 - 2014.0
TUCN	121.49613	24.57484	38.4 ± 0.6	-3.4 ± 0.4	10.5 ± 3.2	2007.0 - 2014.0
TUNH	121.30022	23.07516	-13.1 ± 0.7	28.3 ± 0.4	0.5 ± 1.9	2007.0 - 2014.0
TUNM	121.49358	23.96521	11.5 ± 0.8	3.3 ± 0.5	-0.7 ± 3.3	2007.0 - 2014.0
TUNS	120.40404	23.31724	23.6 ± 0.3	-9.6 ± 0.3	-5.8 ± 1.6	2007.0 - 2014.0
W021	120.54951	23.53568	19.0 ± 1.1	-7.3 ± 0.9	-0.1 ± 6.9	2007.0 - 2014.0
W029	120.66425	23.54079	12.9 ± 0.8	-7.6 ± 0.4	0.9 ± 2.5	2007.0 - 2014.0
WANC	120.52633	23.18684	-0.3 ± 0.4	-6.3 ± 0.4	4.5 ± 1.9	2007.1 - 2014.0
WANL	121.63756	25.16938	35.1 ± 0.4	-10.7 ± 0.3	-1.4 ± 1.9	2007.0 - 2014.0

Table 1. (Continued)

Site	Lon. (°)	Lat. (°)	$V_e$ (mm yr <sup>-1</sup> )	$V_n$ (mm yr <sup>-1</sup> )	$V_u$ (mm yr <sup>-1</sup> )	Period (year)
WANS	120.88519	23.60750	1.3 ± 0.4	0.9 ± 0.3	8.2 ± 1.7	2007.0 - 2014.0
WDAN	120.50431	22.60606	-20.9 ± 0.6	-14.5 ± 0.3	-3.1 ± 1.8	2007.1 - 2014.0
WFEN	120.69947	24.04194	25.1 ± 0.3	-8.8 ± 0.2	-3.3 ± 1.2	2007.0 - 2014.0
WIPN	121.05855	24.67463	29.0 ± 0.4	-6.3 ± 0.4	0.4 ± 2.2	2007.0 - 2014.0
WUFN	120.69939	24.04278	25.0 ± 0.3	-9.1 ± 0.2	-3.3 ± 1.3	2007.0 - 2014.0
WUKU	121.40066	25.11728	32.8 ± 0.3	-9.6 ± 0.3	-1.9 ± 1.5	2007.0 - 2014.0
WUST	120.36817	23.20524	20.5 ± 0.5	-10.7 ± 0.3	1.6 ± 1.3	2007.0 - 2014.0
YAME	121.18529	24.90845	31.3 ± 0.3	-8.5 ± 0.2	1.4 ± 1.4	2007.0 - 2014.0
YENC	120.37615	22.76351	-23.1 ± 1.4	-22.3 ± 1.1	-0.7 ± 7.7	2007.0 - 2009.3
YENL	121.60184	23.90350	6.2 ± 0.5	15.6 ± 0.8	-7.6 ± 1.9	2007.0 - 2014.0
YM01	121.53954	25.17888	33.9 ± 0.7	-10.3 ± 0.5	-2.3 ± 3.8	2007.0 - 2014.0
YM02	121.56069	25.14838	34.7 ± 0.5	-11.7 ± 0.5	6.4 ± 3.7	2007.0 - 2014.0
YM03	121.60490	25.14661	35.0 ± 0.5	-11.3 ± 0.4	-2.8 ± 2.0	2007.0 - 2013.9
YM04	121.58547	25.18760	32.3 ± 1.3	-13.3 ± 2.0	5.8 ± 9.1	2007.0 - 2011.0
YM05	121.56548	25.16400	34.8 ± 0.6	-10.7 ± 0.4	-2.4 ± 1.8	2007.0 - 2014.0
YNTS	121.77893	24.86174	35.8 ± 0.4	-11.1 ± 0.4	0.3 ± 1.8	2007.0 - 2014.0
YSAN	120.08598	23.14655	31.7 ± 0.3	-13.3 ± 0.2	-5.6 ± 1.4	2007.0 - 2014.0
YUL1	121.30021	23.32138	3.5 ± 1.8	10.5 ± 1.1	-15.6 ± 8.7	2011.0 - 2014.0
YULI	121.30113	23.34093	0.1 ± 1.5	13.4 ± 2.4	-11.8 ± 9.0	2007.0 - 2010.9
YUNL	120.79857	23.88388	12.7 ± 0.5	-2.9 ± 0.3	5.1 ± 2.4	2007.0 - 2014.0
YUSN	120.95914	23.48730	-6.8 ± 1.7	-3.4 ± 0.4	-2.5 ± 2.6	2007.0 - 2014.0
ZEND	120.21756	22.94327	18.1 ± 0.4	-13.5 ± 0.4	4.6 ± 2.9	2007.0 - 2014.0
ZWEN	120.49734	23.21974	6.6 ± 0.3	-11.6 ± 0.3	9.8 ± 1.5	2007.0 - 2014.0

Table 2. Velocities of cGPS stations in the Taiwan area w.r.t. Paisha, Penghu (2007 - 2013).

Site	Lon. (°)	Lat. (°)	$V_h$ (mm yr <sup>-1</sup> )	Azi (°)	$V_u$ (mm yr <sup>-1</sup> )	Period (year)
8118	120.55298	23.46298	15.7 ± 0.6	285.5 ± 1.8	0.5 ± 3.0	2007.0 - 2014.0
AKND	120.35726	22.80331	40.7 ± 1.0	256.2 ± 0.5	2.7 ± 1.4	2007.0 - 2014.0
ALIS	120.81329	23.50817	29.2 ± 0.5	281.5 ± 0.8	0.5 ± 1.6	2007.3 - 2014.0
ANKN	121.52472	24.95910	3.7 ± 0.4	34.1 ± 4.6	-2.3 ± 1.5	2007.0 - 2014.0
BALN	121.42612	24.69948	9.4 ± 0.5	342.0 ± 2.4	-1.5 ± 1.8	2007.0 - 2014.0
BANC	121.44210	24.99765	3.3 ± 0.5	28.9 ± 5.6	-1.6 ± 1.8	2007.0 - 2014.0
BANP	120.30540	22.69313	55.0 ± 1.7	242.8 ± 1.3	2.1 ± 6.2	2007.3 - 2013.2
BLOW	121.57124	24.17175	10.5 ± 0.7	303.7 ± 2.7	1.3 ± 2.9	2007.0 - 2014.0
C001	120.61239	23.41794	25.5 ± 0.6	286.9 ± 1.1	2.0 ± 2.0	2007.0 - 2014.0
C002	120.57719	23.36174	26.1 ± 0.5	284.2 ± 0.9	3.9 ± 1.8	2007.0 - 2014.0
CHEN	121.37358	23.09740	68.6 ± 0.4	309.4 ± 0.2	-1.6 ± 1.6	2007.0 - 2014.0
CHIA	120.43320	23.49597	9.3 ± 0.4	290.8 ± 1.8	-2.3 ± 1.4	2007.0 - 2014.0
CHIH	121.20598	23.11584	38.8 ± 0.9	297.6 ± 0.7	-4.5 ± 3.0	2007.0 - 2014.0
CHIN	120.58215	24.27101	0.7 ± 1.2	206.6 ± 65.7	3.5 ± 5.0	2007.0 - 2014.0
CHIU	120.82890	23.94538	21.4 ± 0.7	303.5 ± 1.1	1.9 ± 1.9	2007.1 - 2014.0
CHKU	120.09275	23.05584	2.3 ± 0.3	250.0 ± 4.9	-4.0 ± 1.1	2007.0 - 2014.0
CHNL	120.56347	23.37714	21.3 ± 4.7	300.8 ± 8.9	-5.5 ± 16.6	2007.8 - 2009.6
CHNT	121.66189	24.14921	10.9 ± 0.8	285.9 ± 3.1	-2.4 ± 3.1	2007.0 - 2014.0
CHUA	120.55730	24.06605	1.9 ± 0.5	304.5 ± 10.9	-6.2 ± 2.6	2007.0 - 2014.0
CHUK	120.60472	23.43871	17.5 ± 1.5	285.2 ± 3.3	5.8 ± 6.7	2011.0 - 2014.0
CHUL	121.12568	23.13236	35.5 ± 0.8	294.1 ± 0.7	2.9 ± 2.5	2007.0 - 2014.0
CHUN	121.39310	23.45285	60.3 ± 0.6	311.4 ± 0.4	-6.0 ± 1.7	2007.0 - 2014.0
CHYN	120.29080	23.39327	4.8 ± 0.4	282.0 ± 2.5	-6.3 ± 1.8	2007.0 - 2014.0

Note: Lon. and Lat. are the longitude and latitude of GPS sites;  $V_h$  and  $V_u$  are the horizontal and vertical components of station velocities with standard errors, respectively; Azi is the azimuth of the horizontal velocity with standard errors; period shows the start and end time of observation period.

Table 2. (Continued)

Site	Lon. (°)	Lat. (°)	$V_h$ (mm yr <sup>-1</sup> )	Azi (°)	$V_u$ (mm yr <sup>-1</sup> )	Period (year)
CLAN	121.51200	24.60225	6.6 ± 0.4	30.8 ± 2.6	2.9 ± 2.0	2007.0 - 2014.0
CLON	120.57960	22.43005	56.0 ± 0.4	269.7 ± 0.3	-16.3 ± 3.2	2007.0 - 2014.0
CTOU	120.27784	22.75468	41.0 ± 0.6	252.3 ± 0.6	-3.6 ± 2.0	2007.0 - 2014.0
CWEN	120.45276	23.47304	10.9 ± 0.4	294.9 ± 1.6	-1.8 ± 1.3	2007.0 - 2014.0
DAHU	120.87183	24.42288	5.5 ± 0.6	298.4 ± 5.0	-2.8 ± 1.5	2007.0 - 2014.0
DAJN	120.86497	22.31130	44.9 ± 0.5	288.2 ± 0.4	0.5 ± 1.7	2007.0 - 2014.0
DANL	120.75191	22.20413	48.0 ± 1.6	279.1 ± 1.3	-0.1 ± 5.9	2010.2 - 2014.0
DASI	120.94441	22.47842	37.9 ± 3.9	288.0 ± 3.3	18.2 ± 10.2	2007.0 - 2011.0
DCHU	121.28057	23.21318	59.3 ± 0.5	311.4 ± 0.3	3.4 ± 2.1	2007.0 - 2014.0
DNFU	121.48228	23.68512	45.9 ± 1.1	306.3 ± 1.0	-7.4 ± 2.8	2007.0 - 2014.0
DONA	120.70351	22.91562	54.6 ± 0.5	271.6 ± 0.3	6.9 ± 1.7	2007.0 - 2014.0
DPIN	120.93280	24.04308	22.5 ± 0.4	297.8 ± 0.6	1.5 ± 1.7	2007.0 - 2014.0
DSIN	121.39803	23.63121	35.9 ± 0.8	305.2 ± 0.8	-8.1 ± 3.0	2007.0 - 2014.0
DULI	121.33059	23.02566	65.2 ± 1.3	312.3 ± 0.8	8.1 ± 4.0	2007.0 - 2014.0
ERLN	120.41955	23.79759	1.5 ± 0.9	356.2 ± 30.4	-11.8 ± 3.3	2007.0 - 2014.0
ERPN	121.16611	22.94217	66.4 ± 0.4	306.4 ± 0.3	5.2 ± 2.0	2007.0 - 2014.0
FENP	121.51942	23.59845	65.4 ± 0.9	313.3 ± 0.5	-4.8 ± 2.9	2007.0 - 2014.0
FIVE	121.78107	25.07105	4.1 ± 0.5	76.0 ± 5.5	-1.7 ± 1.2	2007.0 - 2014.0
FKDO	120.85627	23.68355	28.3 ± 2.8	298.7 ± 3.4	-8.5 ± 12.0	2007.0 - 2011.0
FLON	121.93748	25.02037	4.4 ± 0.8	105.9 ± 8.9	-3.4 ± 2.0	2007.0 - 2014.0
FNGU	120.72445	24.03516	11.1 ± 0.4	296.8 ± 1.2	-2.5 ± 1.2	2007.0 - 2014.0
FUNY	120.32017	23.92231	1.4 ± 0.4	45.0 ± 10.3	-13.2 ± 2.9	2007.0 - 2014.0
FUQE	120.82331	24.01115	16.1 ± 0.6	304.1 ± 1.3	-1.3 ± 2.1	2008.4 - 2014.0
FUSN	121.33146	24.79904	6.1 ± 0.6	0.9 ± 3.8	0.3 ± 2.1	2007.3 - 2014.0
GAIS	120.59062	23.08029	40.8 ± 0.5	275.2 ± 0.4	8.5 ± 1.8	2007.0 - 2014.0
GS01	121.50816	24.98200	5.3 ± 0.6	31.9 ± 4.3	0.7 ± 1.7	2007.0 - 2014.0
GS02	120.98234	24.80972	2.9 ± 0.5	310.8 ± 6.8	-3.9 ± 1.5	2007.0 - 2014.0
GS03	121.04407	24.77660	4.3 ± 0.8	339.4 ± 8.0	-1.6 ± 1.4	2007.0 - 2014.0
GS04	120.50679	23.59152	6.6 ± 1.3	297.0 ± 7.3	-1.3 ± 5.2	2007.0 - 2009.9
GS05	120.56840	23.56711	14.0 ± 0.4	290.1 ± 0.9	-0.1 ± 1.4	2007.0 - 2014.0
GS06	120.55422	23.46561	15.6 ± 0.4	283.0 ± 1.1	0.8 ± 1.4	2007.0 - 2014.0
GS07	120.65483	23.48291	19.8 ± 0.4	285.8 ± 0.9	3.6 ± 1.6	2007.0 - 2014.0
GS08	121.50149	25.20373	2.8 ± 0.8	22.9 ± 10.5	-1.7 ± 2.0	2007.0 - 2014.0
GS09	121.65193	25.20861	3.5 ± 0.4	66.4 ± 4.9	-0.3 ± 1.6	2007.0 - 2014.0
GS10	121.46155	25.14615	2.1 ± 0.6	315.0 ± 12.2	-5.8 ± 1.9	2007.0 - 2014.0
GS11	121.49877	25.13357	2.6 ± 0.5	357.8 ± 8.8	-3.7 ± 1.8	2007.0 - 2014.0
GS12	121.38276	25.05303	3.5 ± 0.5	21.5 ± 6.3	0.6 ± 1.7	2007.0 - 2014.0
GS13	121.45224	25.02001	3.7 ± 0.7	34.1 ± 8.3	-6.3 ± 3.2	2007.0 - 2014.0
GS14	120.95945	24.80322	2.9 ± 0.3	350.2 ± 3.9	-1.9 ± 1.2	2007.0 - 2014.0
GS15	120.99050	24.76665	3.8 ± 0.3	341.6 ± 3.0	-0.7 ± 1.2	2007.0 - 2014.0
GS16	121.04161	24.74787	4.6 ± 0.4	339.6 ± 3.6	-0.4 ± 1.3	2007.0 - 2014.0
GS17	120.60584	23.56115	17.8 ± 0.4	288.6 ± 1.0	1.9 ± 1.5	2007.0 - 2014.0
GS18	120.47378	23.48498	10.9 ± 0.4	287.1 ± 1.6	-1.0 ± 1.2	2007.0 - 2014.0
GS19	121.67981	25.07174	4.6 ± 0.6	73.5 ± 6.2	-0.6 ± 2.2	2007.0 - 2012.4
GS20	121.94321	24.84190	15.3 ± 0.7	121.6 ± 2.1	-19.3 ± 1.7	2007.0 - 2014.0
GS21	120.51241	24.09648	1.5 ± 0.3	293.2 ± 7.5	-3.1 ± 1.3	2007.0 - 2014.0
GS22	120.60390	24.09133	3.4 ± 0.3	298.1 ± 3.4	-3.6 ± 1.3	2007.0 - 2014.0
GS23	120.64816	24.09370	4.3 ± 0.4	302.6 ± 3.1	-2.1 ± 1.8	2007.0 - 2014.0
GS24	120.52644	24.02564	1.9 ± 0.4	295.2 ± 6.8	-8.1 ± 2.1	2007.0 - 2014.0
GS25	120.64059	23.98667	4.6 ± 0.4	299.9 ± 3.7	-3.9 ± 1.9	2007.0 - 2014.0
GS26	120.57870	23.82489	4.8 ± 0.4	294.4 ± 2.6	-1.9 ± 1.6	2007.0 - 2014.0
GS27	120.64631	23.87021	4.1 ± 0.4	299.1 ± 3.2	-2.2 ± 1.8	2007.0 - 2014.0

Table 2. (Continued)

Site	Lon. (°)	Lat. (°)	$V_h$ (mm yr <sup>-1</sup> )	Azi (°)	$V_u$ (mm yr <sup>-1</sup> )	Period (year)
GS28	120.21358	23.07986	5.4 ± 0.6	270.0 ± 3.2	-3.8 ± 2.9	2007.0 - 2014.0
GS29	120.31755	23.07537	10.1 ± 0.5	265.5 ± 1.7	2.7 ± 1.3	2007.0 - 2014.0
GS30	120.22612	23.02032	11.4 ± 0.4	270.0 ± 1.5	0.2 ± 1.3	2007.0 - 2014.0
GS31	120.27588	23.01875	15.9 ± 0.5	265.3 ± 0.7	-2.5 ± 1.3	2007.0 - 2014.0
GS32	120.33584	23.02714	19.9 ± 0.6	259.0 ± 0.9	1.2 ± 1.3	2007.0 - 2014.0
GS33	120.18695	22.96369	10.7 ± 0.4	268.9 ± 1.1	-3.0 ± 1.2	2007.0 - 2014.0
GS34	120.27632	22.93612	23.0 ± 0.6	267.0 ± 0.5	3.1 ± 1.3	2007.0 - 2014.0
GS35	120.30849	22.93581	23.6 ± 0.5	264.4 ± 0.5	4.1 ± 1.6	2007.0 - 2014.0
GS36	120.62530	24.36200	2.1 ± 0.4	307.4 ± 6.5	-2.3 ± 1.2	2007.0 - 2014.0
GS37	120.71540	24.32860	4.4 ± 0.4	298.3 ± 3.9	-2.9 ± 1.3	2007.0 - 2014.0
GS38	120.60060	24.27980	1.6 ± 0.4	291.8 ± 7.7	-3.2 ± 1.3	2007.0 - 2014.0
GS39	120.52960	24.18440	1.5 ± 0.4	306.9 ± 9.2	-2.9 ± 1.2	2007.0 - 2014.0
GS40	120.57630	24.18120	2.5 ± 0.4	316.6 ± 5.8	-2.9 ± 1.1	2007.0 - 2014.0
GS41	120.44490	23.37760	10.8 ± 0.6	288.3 ± 2.6	-4.3 ± 2.1	2007.9 - 2014.0
GS42	120.45200	23.27320	18.4 ± 0.5	278.7 ± 0.9	4.5 ± 1.7	2007.9 - 2014.0
GS43	120.37360	23.25720	8.5 ± 0.5	282.9 ± 2.1	-1.7 ± 1.7	2007.9 - 2014.0
GS44	120.40040	23.22220	15.3 ± 0.4	273.0 ± 1.1	5.8 ± 1.7	2007.9 - 2014.0
GS45	120.72800	22.75250	57.3 ± 0.9	272.7 ± 0.6	8.5 ± 4.2	2009.0 - 2014.0
GS46	120.63950	22.52970	57.1 ± 0.8	271.4 ± 0.6	2.6 ± 4.4	2009.0 - 2014.0
GS47	120.73700	21.95060	37.8 ± 2.4	278.8 ± 1.6	-30.6 ± 5.0	2009.0 - 2013.6
GS51	120.54006	23.00022	47.7 ± 0.9	266.6 ± 0.7	6.0 ± 3.3	2010.0 - 2014.0
GS52	120.65472	23.03402	50.1 ± 0.9	270.8 ± 0.7	6.0 ± 3.5	2010.0 - 2014.0
GS53	120.39831	22.83998	42.2 ± 0.9	259.6 ± 0.8	8.0 ± 4.1	2010.0 - 2014.0
GS54	120.45209	22.83710	53.8 ± 1.1	265.2 ± 0.7	-0.1 ± 4.0	2010.0 - 2013.5
GS55	120.60224	22.85069	56.1 ± 1.1	270.7 ± 0.8	2.2 ± 3.5	2009.9 - 2014.0
GS56	120.60173	22.70388	57.3 ± 1.0	269.3 ± 0.6	1.0 ± 4.0	2010.0 - 2014.0
GS57	120.76485	22.12753	47.1 ± 1.6	279.9 ± 1.0	1.3 ± 4.8	2010.0 - 2014.0
GS58	120.83892	22.12637	43.2 ± 1.2	289.2 ± 1.0	-2.6 ± 5.0	2010.0 - 2014.0
GS59	120.70439	22.05740	49.3 ± 1.1	269.5 ± 0.8	-3.4 ± 4.2	2010.0 - 2014.0
GS60	120.80973	22.00754	43.4 ± 1.6	287.6 ± 1.2	1.1 ± 5.2	2010.0 - 2014.0
GS61	121.20048	24.67880	8.2 ± 1.4	341.6 ± 8.1	0.5 ± 6.5	2010.8 - 2014.0
GS62	121.24302	24.73348	7.8 ± 1.3	352.6 ± 8.1	0.3 ± 5.1	2010.8 - 2014.0
GS63	120.62683	23.54326	18.3 ± 2.2	285.9 ± 5.8	4.2 ± 4.4	2010.7 - 2014.0
GS64	120.71215	23.40764	30.1 ± 1.2	279.2 ± 1.5	4.0 ± 4.7	2010.7 - 2014.0
GS66	120.74150	23.45619	28.9 ± 1.3	279.4 ± 1.8	6.2 ± 4.5	2010.7 - 2014.0
GS67	120.67515	23.33968	30.4 ± 1.1	281.8 ± 1.3	4.0 ± 4.3	2010.7 - 2014.0
GS68	120.48770	23.60710	7.7 ± 1.4	280.4 ± 5.4	-5.3 ± 6.3	2011.0 - 2014.0
GS69	121.37797	24.96777	3.5 ± 2.4	50.8 ± 27.5	1.0 ± 11.4	2011.7 - 2014.0
GUKN	120.58878	23.64586	9.1 ± 0.4	304.7 ± 1.8	-1.1 ± 2.0	2007.0 - 2014.0
GUKW	121.00655	24.20220	19.0 ± 0.6	308.4 ± 1.3	2.3 ± 3.8	2007.0 - 2014.0
HANS	121.68714	24.60951	19.6 ± 0.8	94.1 ± 2.0	-1.9 ± 2.1	2007.0 - 2014.0
HENC	120.74645	22.00393	51.7 ± 0.8	271.6 ± 0.4	-5.6 ± 2.2	2007.0 - 2014.0
HERI	121.58092	25.29444	2.2 ± 0.5	39.5 ± 9.4	-0.6 ± 1.6	2007.0 - 2014.0
HLIU	120.99417	23.79303	35.1 ± 1.0	294.4 ± 1.1	1.1 ± 3.3	2007.0 - 2014.0
HOKN	120.13488	23.18838	1.9 ± 0.3	261.0 ± 6.0	-7.5 ± 1.3	2007.0 - 2014.0
HOPN	120.89488	24.17078	17.2 ± 0.9	297.0 ± 2.5	-9.7 ± 3.3	2007.0 - 2014.0
HRGN	121.40510	23.55528	49.9 ± 0.6	307.7 ± 0.5	-12.7 ± 2.4	2007.0 - 2014.0
HSIN	121.01425	24.82775	2.4 ± 0.4	345.4 ± 7.1	-1.6 ± 1.3	2007.0 - 2014.0
HSUE	121.02645	24.28059	19.9 ± 0.9	306.6 ± 1.7	-3.8 ± 2.6	2007.0 - 2014.0
HUAL	121.61351	23.97538	27.6 ± 0.7	302.7 ± 1.0	-7.0 ± 2.1	2007.0 - 2014.0
HUAN	121.27262	24.14347	23.2 ± 1.1	313.6 ± 1.9	0.6 ± 1.8	2007.1 - 2014.0
HUAP	121.74944	24.30900	12.3 ± 0.9	158.0 ± 3.2	-3.0 ± 3.2	2007.0 - 2014.0

Table 2. (Continued)

Site	Lon. (°)	Lat. (°)	$V_h$ (mm yr <sup>-1</sup> )	Azi (°)	$V_u$ (mm yr <sup>-1</sup> )	Period (year)
HUWE	120.28662	23.72940	2.0 ± 0.3	339.8 ± 5.7	-30.2 ± 2.7	2007.0 - 2014.0
HUYA	121.02941	24.09233	25.4 ± 0.5	296.0 ± 0.7	6.0 ± 1.6	2007.0 - 2014.0
ICHU	120.27930	23.36066	5.1 ± 0.4	283.5 ± 3.3	-10.5 ± 1.5	2007.0 - 2014.0
ILAN	121.75662	24.76404	8.8 ± 0.4	117.7 ± 2.0	-8.4 ± 1.7	2007.0 - 2014.0
JLUT	120.62278	22.32996	53.7 ± 0.6	271.6 ± 0.4	-0.1 ± 1.9	2007.0 - 2014.0
JONP	120.52400	23.42297	14.5 ± 0.4	288.9 ± 1.2	2.2 ± 1.3	2007.0 - 2014.0
JPEI	121.37139	23.53160	35.9 ± 0.9	309.0 ± 0.9	-4.5 ± 2.6	2007.0 - 2014.0
JPIN	121.35889	23.34108	61.0 ± 0.5	316.1 ± 0.3	6.5 ± 1.8	2007.0 - 2014.0
JSUI	121.42389	23.49198	60.4 ± 0.7	313.0 ± 0.4	-0.7 ± 2.7	2007.0 - 2014.0
JYAN	121.22634	24.24247	20.0 ± 0.7	332.7 ± 1.4	3.3 ± 1.8	2007.0 - 2014.0
KASU	120.63298	22.81019	58.0 ± 1.1	268.6 ± 0.8	3.7 ± 2.6	2007.3 - 2014.0
KNKO	121.50574	23.47221	67.6 ± 0.4	314.2 ± 0.3	-6.4 ± 2.0	2007.0 - 2014.0
KSHI	121.17603	24.77666	5.3 ± 1.0	335.4 ± 9.2	-4.9 ± 8.2	2007.0 - 2014.0
KUAN	121.16425	23.04968	34.0 ± 0.9	296.0 ± 1.0	-6.0 ± 3.1	2007.0 - 2014.0
KULN	120.50702	23.33098	23.4 ± 0.5	279.8 ± 0.7	6.5 ± 1.5	2007.0 - 2014.0
KYIN	121.08042	25.04105	2.0 ± 0.4	342.5 ± 8.4	0.9 ± 1.3	2007.0 - 2014.0
KZN1	120.69798	23.94625	6.9 ± 0.4	292.9 ± 1.8	-4.8 ± 1.6	2007.0 - 2014.0
LAIG	120.73990	23.52940	27.1 ± 0.7	280.6 ± 1.1	4.2 ± 2.6	2008.6 - 2014.0
LANY	121.55810	22.03731	82.7 ± 1.0	303.5 ± 0.5	1.1 ± 1.9	2007.0 - 2014.0
LAOL	120.68729	22.41192	54.0 ± 1.5	271.6 ± 0.8	1.7 ± 4.9	2007.0 - 2012.0
LGUE	120.63538	22.99290	50.5 ± 0.8	269.5 ± 0.5	9.3 ± 3.1	2007.0 - 2014.0
LIKU	120.52790	22.75861	58.5 ± 0.9	264.4 ± 0.6	4.1 ± 4.3	2007.0 - 2014.0
LIUC	120.36907	22.34667	58.5 ± 1.3	243.3 ± 0.7	-1.7 ± 4.3	2007.0 - 2013.9
LIYU	120.78180	24.34306	1.8 ± 0.9	260.5 ± 15.9	7.7 ± 3.2	2007.0 - 2014.0
LNCH	120.40261	22.99458	24.6 ± 0.5	254.2 ± 0.5	12.1 ± 1.3	2007.0 - 2014.0
LNKO	121.37818	25.07637	3.7 ± 0.4	22.4 ± 5.9	-0.5 ± 2.3	2007.0 - 2014.0
LONT	121.13056	22.90631	44.4 ± 1.0	298.0 ± 1.1	3.6 ± 2.1	2007.0 - 2014.0
LOYE	120.70120	23.46860	24.6 ± 0.7	283.4 ± 1.2	0.9 ± 2.2	2008.6 - 2014.0
LSAN	121.18216	24.02934	25.7 ± 0.6	297.4 ± 0.9	6.4 ± 1.7	2007.0 - 2014.0
LTUN	121.77162	24.70003	14.1 ± 0.5	116.9 ± 1.3	-7.1 ± 2.1	2007.0 - 2014.0
LUGU	120.74769	23.75226	20.5 ± 1.2	294.8 ± 2.3	2.0 ± 6.4	2007.0 - 2010.2
LUKN	120.43513	24.06001	2.1 ± 0.4	286.7 ± 5.8	-6.6 ± 1.9	2007.0 - 2014.0
LUSN	121.18605	24.03519	25.9 ± 1.2	293.4 ± 1.5	0.9 ± 3.4	2007.1 - 2014.0
MATZ	119.92306	26.16939	1.1 ± 0.4	236.3 ± 12.5	-1.0 ± 1.1	2007.0 - 2014.0
MESN	120.82626	23.26363	33.5 ± 0.6	276.7 ± 0.5	7.8 ± 2.2	2007.0 - 2014.0
MFEN	121.17247	24.08216	32.7 ± 0.6	300.3 ± 0.6	3.8 ± 1.3	2007.0 - 2014.0
MIAO	120.81026	24.58345	4.4 ± 0.5	303.0 ± 4.3	-1.2 ± 1.7	2007.0 - 2014.0
MINS	120.72090	23.27540	32.8 ± 0.8	280.9 ± 1.0	5.7 ± 2.6	2007.0 - 2012.0
MITO	120.26315	22.79585	25.6 ± 1.6	254.8 ± 2.3	-0.8 ± 5.5	2007.0 - 2012.5
MLO1	120.55400	22.90000	50.9 ± 0.8	265.7 ± 0.5	-2.2 ± 3.0	2007.0 - 2012.0
MOTN	121.02685	23.20054	33.2 ± 0.8	281.5 ± 0.7	3.1 ± 2.4	2007.0 - 2014.0
NAAO	121.81021	24.44934	19.0 ± 0.8	152.4 ± 1.6	-9.0 ± 1.8	2007.0 - 2014.0
NANK	120.27439	23.10199	5.9 ± 0.4	264.2 ± 1.9	-2.1 ± 1.5	2007.0 - 2014.0
NCKU	120.27581	22.93845	23.5 ± 0.5	267.6 ± 0.5	2.7 ± 1.5	2007.0 - 2014.0
NDHU	121.55081	23.89724	33.5 ± 0.8	302.9 ± 1.0	-6.1 ± 1.9	2007.0 - 2014.0
NEMN	120.42008	22.90812	38.3 ± 0.5	262.7 ± 0.5	7.8 ± 1.9	2007.0 - 2014.0
NHSI	121.45301	23.40621	64.6 ± 0.7	315.8 ± 0.5	-3.0 ± 2.7	2007.0 - 2014.0
NIUT	121.56158	24.63478	8.3 ± 0.8	45.0 ± 4.1	3.2 ± 4.0	2007.0 - 2014.0
NJOU	120.57141	22.50389	57.2 ± 0.6	269.1 ± 0.4	-11.8 ± 2.6	2007.0 - 2014.0
NSAN	121.38280	24.42820	11.3 ± 0.9	341.4 ± 3.5	7.1 ± 2.9	2007.0 - 2014.0
NSHE	120.80090	24.22579	11.5 ± 0.4	294.1 ± 1.5	0.8 ± 1.6	2007.0 - 2014.0
PAKU	120.63603	23.91568	4.8 ± 0.4	290.7 ± 2.8	-2.3 ± 1.7	2007.0 - 2014.0

Table 2. (Continued)

Site	Lon. (°)	Lat. (°)	$V_h$ (mm yr <sup>-1</sup> )	Azi (°)	$V_u$ (mm yr <sup>-1</sup> )	Period (year)
PANG	119.56374	23.56520	0.8 ± 0.3	104.0 ± 13.9	-1.1 ± 1.5	2007.0 - 2014.0
PAOL	120.70287	23.10862	44.5 ± 0.9	273.5 ± 0.6	12.7 ± 1.7	2007.0 - 2014.0
PAOS	120.95028	24.71492	5.3 ± 0.6	339.2 ± 5.2	0.9 ± 1.7	2007.0 - 2014.0
PEI1	120.16900	23.29400	5.8 ± 1.3	251.9 ± 7.4	-14.0 ± 4.9	2007.0 - 2014.0
PEIN	121.12313	22.80107	48.5 ± 0.6	281.4 ± 0.5	1.8 ± 2.2	2007.2 - 2013.9
PENL	120.97604	24.53884	9.7 ± 2.1	324.7 ± 9.2	-2.2 ± 7.1	2007.0 - 2014.0
PEPU	121.61034	24.01788	19.9 ± 1.0	296.2 ± 2.2	-5.5 ± 2.6	2007.0 - 2014.0
PING	121.45434	23.31946	68.0 ± 0.5	314.6 ± 0.3	-1.3 ± 1.9	2007.0 - 2014.0
PINT	120.64056	23.75606	4.5 ± 0.5	305.1 ± 4.3	-4.0 ± 1.3	2007.0 - 2014.0
PLAN	121.08660	24.57895	9.0 ± 0.6	353.0 ± 3.2	-1.4 ± 2.3	2007.0 - 2014.0
PLIN	121.71395	24.93362	1.7 ± 0.9	54.5 ± 21.2	3.5 ± 3.2	2007.0 - 2014.0
PNCY	122.07944	25.62750	1.1 ± 0.7	37.9 ± 26.8	-2.3 ± 3.1	2009.0 - 2013.4
PTUN	120.45968	22.64985	57.5 ± 0.9	260.2 ± 0.5	5.8 ± 3.7	2007.0 - 2014.0
PUSN	120.52011	23.96494	1.1 ± 2.2	248.2 ± 76.9	-8.8 ± 6.1	2007.0 - 2014.0
RENI	120.50857	23.45894	13.3 ± 0.4	285.3 ± 1.3	0.8 ± 1.3	2007.0 - 2014.0
S011	120.33945	23.20542	8.5 ± 0.8	276.8 ± 4.1	0.0 ± 1.4	2007.0 - 2014.0
S012	120.48826	23.05947	34.7 ± 0.5	273.5 ± 0.5	4.8 ± 1.5	2007.0 - 2014.0
S016	120.80286	24.17955	13.0 ± 0.4	285.2 ± 1.3	-1.3 ± 1.2	2007.0 - 2014.0
S101	121.61385	25.04045	3.1 ± 0.4	50.2 ± 5.5	-2.1 ± 1.5	2007.0 - 2014.0
S102	121.55815	22.03721	84.3 ± 2.2	305.3 ± 1.1	0.4 ± 5.7	2007.0 - 2010.8
S103	120.47519	23.56437	7.8 ± 0.4	299.8 ± 1.7	-1.6 ± 1.3	2007.0 - 2014.0
S104	121.18938	22.82076	67.8 ± 0.5	307.1 ± 0.3	1.5 ± 1.5	2007.0 - 2014.0
S105	121.11289	22.95165	33.7 ± 0.5	293.1 ± 0.5	-4.1 ± 1.6	2007.0 - 2014.0
S106	120.33409	23.05079	16.9 ± 0.6	261.5 ± 1.7	2.4 ± 1.2	2007.0 - 2014.0
S167	120.93410	23.95442	23.4 ± 0.4	297.4 ± 0.6	1.6 ± 1.4	2007.0 - 2014.0
S169	120.50331	22.94229	46.5 ± 0.5	269.4 ± 0.4	-0.5 ± 1.6	2007.0 - 2014.0
S170	120.76763	23.74596	24.6 ± 0.4	293.0 ± 0.5	0.5 ± 1.4	2007.0 - 2014.0
S23R	120.60617	22.64498	55.3 ± 0.5	270.3 ± 0.3	1.4 ± 2.0	2007.0 - 2014.0
SALU	120.57830	24.14445	2.4 ± 0.4	311.6 ± 5.9	-1.4 ± 1.5	2007.0 - 2014.0
SAND	120.64064	22.71727	57.9 ± 0.6	270.7 ± 0.4	3.6 ± 1.9	2007.0 - 2014.0
SANI	120.76873	24.41435	4.3 ± 0.6	327.4 ± 6.3	-15.6 ± 7.4	2007.0 - 2014.0
SANJ	121.50087	25.26079	1.5 ± 0.4	23.2 ± 11.3	-3.1 ± 1.9	2007.0 - 2014.0
SANL	120.76855	23.66448	25.9 ± 0.6	295.9 ± 0.9	1.6 ± 1.4	2007.0 - 2014.0
SCHN	121.65159	24.12779	13.8 ± 1.0	289.1 ± 2.6	-1.3 ± 3.7	2008.8 - 2014.0
SFON	121.01016	24.93289	1.1 ± 0.5	338.2 ± 20.6	-4.2 ± 1.6	2007.0 - 2014.0
SGAN	120.34965	22.58127	50.0 ± 0.6	247.3 ± 0.5	-1.8 ± 1.7	2007.0 - 2014.0
SGUN	120.69188	24.27163	4.1 ± 0.4	297.8 ± 3.2	-3.7 ± 1.4	2007.0 - 2014.0
SHAN	121.19949	23.10886	34.9 ± 0.6	301.9 ± 0.6	-7.7 ± 2.3	2007.0 - 2014.0
SHUL	121.56273	23.78761	43.2 ± 0.6	318.4 ± 0.6	-11.1 ± 2.1	2007.0 - 2014.0
SHWA	120.34781	23.02143	20.8 ± 0.5	259.5 ± 0.6	3.1 ± 1.3	2007.0 - 2014.0
SILN	120.64604	23.16038	35.2 ± 1.7	274.2 ± 1.6	9.1 ± 7.0	2007.0 - 2009.6
SINL	121.25462	22.90829	65.5 ± 0.6	310.0 ± 0.3	0.5 ± 1.8	2007.0 - 2014.0
SJPU	120.48126	23.42854	12.2 ± 0.4	286.2 ± 1.4	-0.9 ± 2.0	2007.0 - 2014.0
SLIN	121.44140	23.81185	27.2 ± 1.1	304.8 ± 1.8	3.9 ± 3.9	2007.0 - 2014.0
SLNP	121.63563	24.75311	4.2 ± 0.4	80.3 ± 4.1	-3.2 ± 1.4	2007.0 - 2014.0
SONA	120.98584	24.39781	10.9 ± 0.5	315.0 ± 1.9	0.1 ± 1.7	2007.5 - 2014.0
SPA0	121.48486	24.20501	12.1 ± 0.7	320.0 ± 2.5	9.7 ± 2.5	2007.0 - 2014.0
SSUN	120.37777	23.41415	9.0 ± 0.4	284.2 ± 1.9	-2.1 ± 1.3	2007.0 - 2014.0
STA1	120.97926	24.63560	4.6 ± 0.7	340.8 ± 6.3	2.6 ± 3.0	2008.1 - 2014.0
SUAB	121.86790	24.59391	32.1 ± 2.0	141.7 ± 2.3	-4.9 ± 4.8	2007.0 - 2011.0
SUAN	120.29988	23.47757	3.9 ± 0.5	283.3 ± 4.5	-6.5 ± 3.2	2007.0 - 2014.0
SUAO	121.86707	24.59239	31.6 ± 0.7	140.9 ± 0.9	-5.1 ± 1.7	2007.0 - 2014.0

Table 2. (Continued)

Site	Lon. (°)	Lat. (°)	$V_h$ (mm yr <sup>-1</sup> )	Azi (°)	$V_u$ (mm yr <sup>-1</sup> )	Period (year)
SUCH	120.90758	24.29107	6.9 ± 1.1	284.2 ± 7.4	7.9 ± 4.1	2007.0 - 2014.0
SUN1	120.90835	23.88124	24.4 ± 0.4	298.3 ± 0.5	1.9 ± 1.5	2007.0 - 2014.0
TAIP	121.67317	25.03452	3.6 ± 0.5	69.1 ± 5.0	-3.2 ± 1.7	2007.2 - 2014.0
TANS	121.42689	25.18150	3.1 ± 2.2	144.2 ± 31.5	4.0 ± 4.4	2007.0 - 2014.0
TAPE	121.23087	23.12557	41.4 ± 0.6	298.9 ± 0.5	-11.3 ± 1.7	2007.0 - 2014.0
TAPO	121.23741	23.12706	62.2 ± 0.7	311.5 ± 0.4	10.3 ± 2.0	2007.0 - 2014.0
TAPU	120.58541	23.25080	31.0 ± 0.6	283.1 ± 0.7	4.9 ± 1.7	2007.0 - 2014.0
TATA	120.88705	23.48140	44.7 ± 0.8	288.6 ± 0.7	2.3 ± 2.5	2007.0 - 2014.0
TEGS	120.65498	24.35621	2.4 ± 0.3	308.3 ± 4.7	-0.1 ± 1.3	2007.0 - 2014.0
TENC	120.91567	23.27779	22.7 ± 2.1	285.9 ± 2.2	-1.8 ± 3.5	2007.0 - 2014.0
THAI	121.29559	24.60712	9.1 ± 0.6	353.0 ± 3.1	2.3 ± 1.5	2007.0 - 2014.0
TMAL	120.95987	22.64892	35.9 ± 0.9	288.5 ± 1.0	0.2 ± 2.1	2007.0 - 2013.9
TOFN	120.92480	24.66204	4.0 ± 0.4	327.1 ± 3.9	-0.1 ± 1.4	2007.0 - 2014.0
TSHI	121.63276	25.25691	2.5 ± 0.5	45.0 ± 8.0	-1.7 ± 2.0	2007.0 - 2014.0
TSIO	120.70410	24.47279	2.5 ± 0.4	315.0 ± 5.7	0.2 ± 1.4	2007.0 - 2014.0
TSLN	120.71938	23.63432	21.2 ± 0.6	289.9 ± 1.3	4.8 ± 2.1	2007.3 - 2012.8
TTSH	121.14762	22.74713	46.1 ± 0.6	286.8 ± 0.5	-6.2 ± 2.9	2008.4 - 2014.0
TTUN	121.08070	22.76455	44.1 ± 0.6	286.3 ± 0.6	-4.6 ± 1.8	2007.0 - 2014.0
TUCN	121.49613	24.57484	10.9 ± 0.7	39.1 ± 2.8	10.0 ± 3.2	2007.0 - 2014.0
TUNH	121.30022	23.07516	60.0 ± 0.8	312.0 ± 0.5	0.0 ± 1.9	2007.0 - 2014.0
TUNM	121.49358	23.96521	25.1 ± 0.9	307.2 ± 1.4	-1.2 ± 3.3	2007.0 - 2014.0
TUNS	120.40404	23.31724	8.2 ± 0.4	286.2 ± 2.1	-6.3 ± 1.6	2007.0 - 2014.0
W021	120.54951	23.53568	13.3 ± 1.4	290.2 ± 4.0	-0.6 ± 6.9	2007.0 - 2014.0
W029	120.66425	23.54079	19.1 ± 0.9	283.0 ± 1.3	0.4 ± 2.5	2007.0 - 2014.0
WANC	120.52633	23.18684	32.3 ± 0.6	280.0 ± 0.7	4.0 ± 1.9	2007.1 - 2014.0
WANL	121.63756	25.16938	3.8 ± 0.5	71.6 ± 4.7	-1.9 ± 1.9	2007.0 - 2014.0
WANS	120.88519	23.60750	32.8 ± 0.5	293.0 ± 0.6	7.7 ± 1.7	2007.0 - 2014.0
WDAN	120.50431	22.60606	52.5 ± 0.7	267.2 ± 0.3	-3.6 ± 1.8	2007.1 - 2014.0
WFEN	120.69947	24.04194	7.1 ± 0.4	295.8 ± 1.8	-3.8 ± 1.2	2007.0 - 2014.0
WIPN	121.05855	24.67463	6.1 ± 0.6	335.9 ± 3.7	-0.1 ± 2.2	2007.0 - 2014.0
WUFN	120.69939	24.04278	7.1 ± 0.4	293.3 ± 1.8	-3.8 ± 1.3	2007.0 - 2014.0
WUKU	121.40066	25.11728	2.6 ± 0.4	29.5 ± 6.5	-2.4 ± 1.5	2007.0 - 2014.0
WUST	120.36817	23.20524	11.1 ± 0.6	276.2 ± 1.6	1.1 ± 1.3	2007.0 - 2014.0
YAME	121.18529	24.90845	3.4 ± 0.4	356.6 ± 5.0	0.9 ± 1.4	2007.0 - 2014.0
YENC	120.37615	22.76351	55.6 ± 1.8	259.2 ± 1.1	-1.2 ± 7.7	2007.0 - 2009.3
YENL	121.60184	23.90350	37.4 ± 0.9	317.4 ± 1.0	-8.1 ± 1.9	2007.0 - 2014.0
YM01	121.53954	25.17888	2.9 ± 0.9	56.3 ± 11.3	-2.8 ± 3.8	2007.0 - 2014.0
YM02	121.56069	25.14838	3.2 ± 0.7	86.4 ± 8.9	5.9 ± 3.7	2007.0 - 2014.0
YM03	121.60490	25.14661	3.6 ± 0.6	80.3 ± 6.5	-3.3 ± 2.0	2007.0 - 2013.9
YM04	121.58547	25.18760	1.6 ± 2.4	150.3 ± 53.4	5.3 ± 9.1	2007.0 - 2011.0
YM05	121.56548	25.16400	3.5 ± 0.7	70.0 ± 7.0	-2.9 ± 1.8	2007.0 - 2014.0
YNTS	121.77893	24.86174	4.4 ± 0.6	79.5 ± 5.2	-0.2 ± 1.8	2007.0 - 2014.0
YSAN	120.08598	23.14655	1.4 ± 0.4	171.9 ± 12.1	-6.1 ± 1.4	2007.0 - 2014.0
YUL1	121.30021	23.32138	35.9 ± 2.1	308.7 ± 2.3	-16.1 ± 8.7	2011.0 - 2014.0
YUL1	121.30113	23.34093	40.3 ± 2.8	308.9 ± 3.0	-12.3 ± 9.0	2007.0 - 2010.9
YUNL	120.79857	23.88388	20.8 ± 0.6	295.6 ± 1.0	4.6 ± 2.4	2007.0 - 2014.0
YUSN	120.95914	23.48730	39.2 ± 1.7	282.5 ± 0.8	-3.0 ± 2.6	2007.0 - 2014.0
ZEND	120.21756	22.94327	13.5 ± 0.6	263.2 ± 1.7	4.1 ± 2.9	2007.0 - 2014.0
ZWEN	120.49734	23.21974	24.9 ± 0.4	270.7 ± 0.7	9.3 ± 1.5	2007.0 - 2014.0

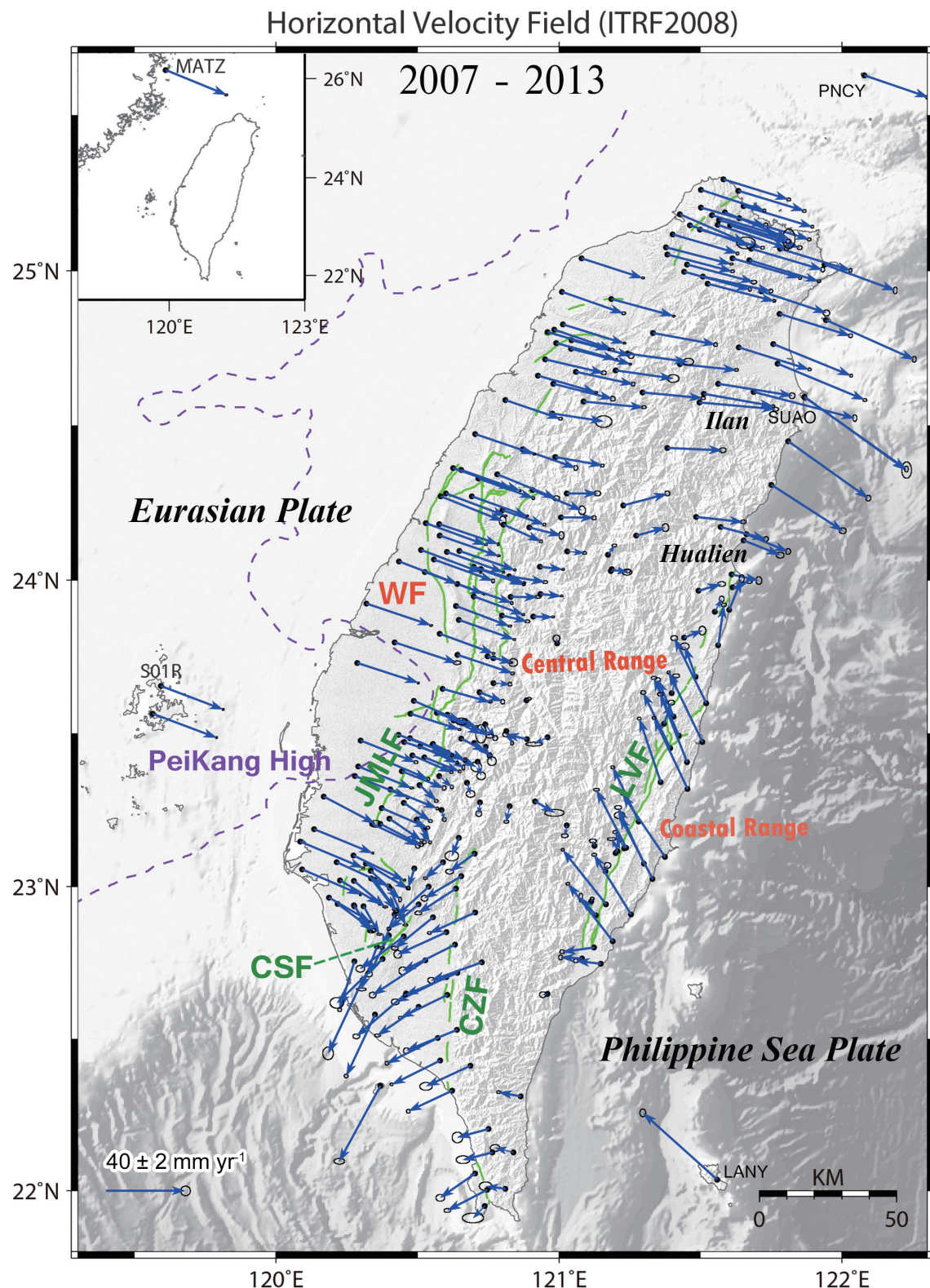


Fig. 19. Horizontal ITRF2008 velocities of cGPS stations in the Taiwan area (2007 - 2013). The green lines indicate the surface traces of active faults. JMLF and LVF denote the Jiuchiunkun-Muchiliao-Liuchia Fault system and Longitude Valley Fault, respectively. CSF and CZF denote the Chishan Fault and Chaozhou Fault, respectively. WF denotes Western Foothills. The blue arrows show velocity vectors. A 95% confidence error ellipse is shown at the tip of each velocity vector. The purple dashed line describes the mirage of Peikang High.

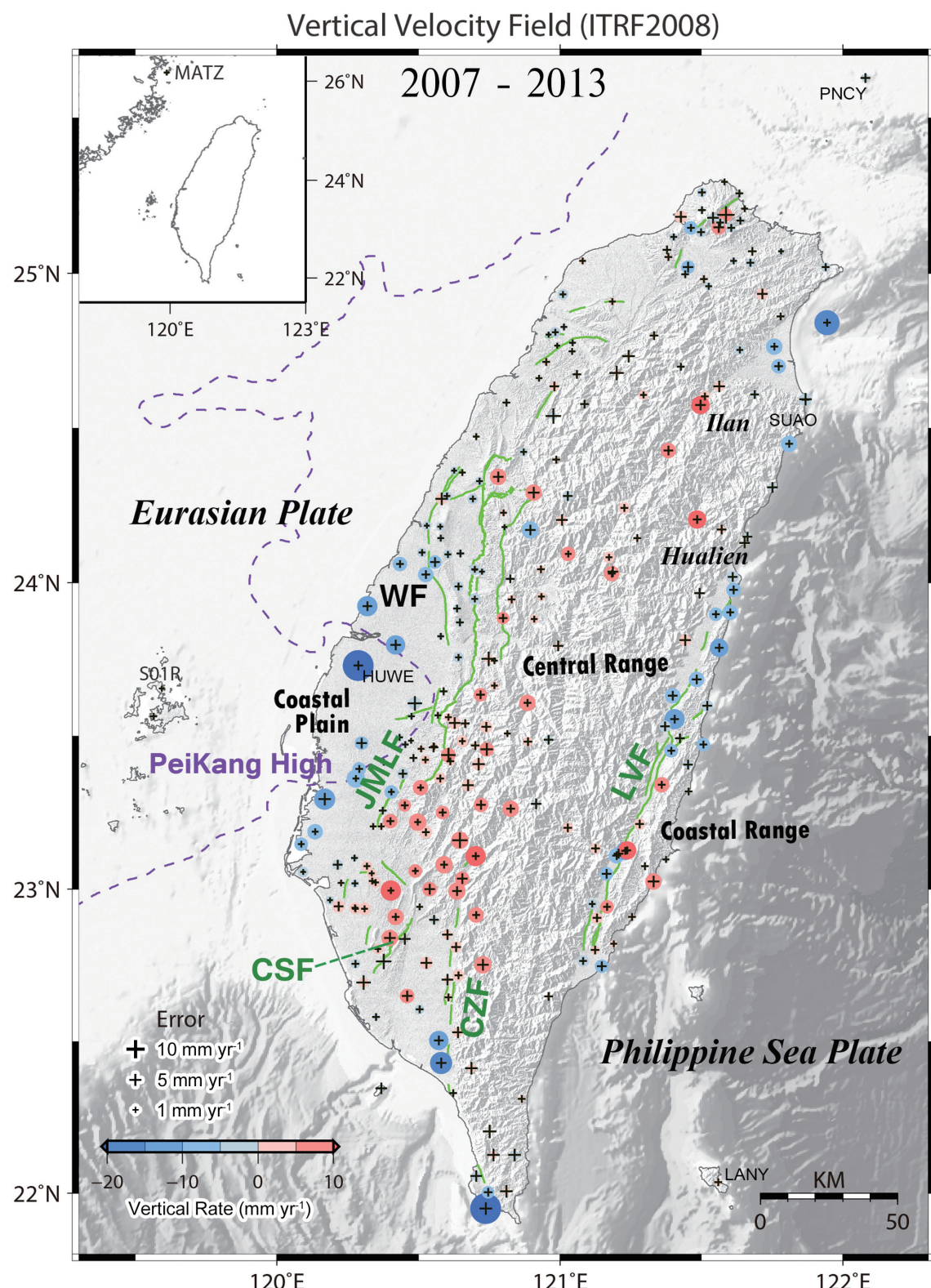


Fig. 20. Vertical ITRF2008 velocities of cGPS stations in the Taiwan area (2007 - 2013). The circle size is proportional to the vertical motion magnitude. JMLF, LVF, CSF, CZF, and WF have the same definition as Fig. 19. Blue circles denote subsidence and red circles denote uplift. The black crosses are STDs and the purple dashed line describes the Peikang High mirage.

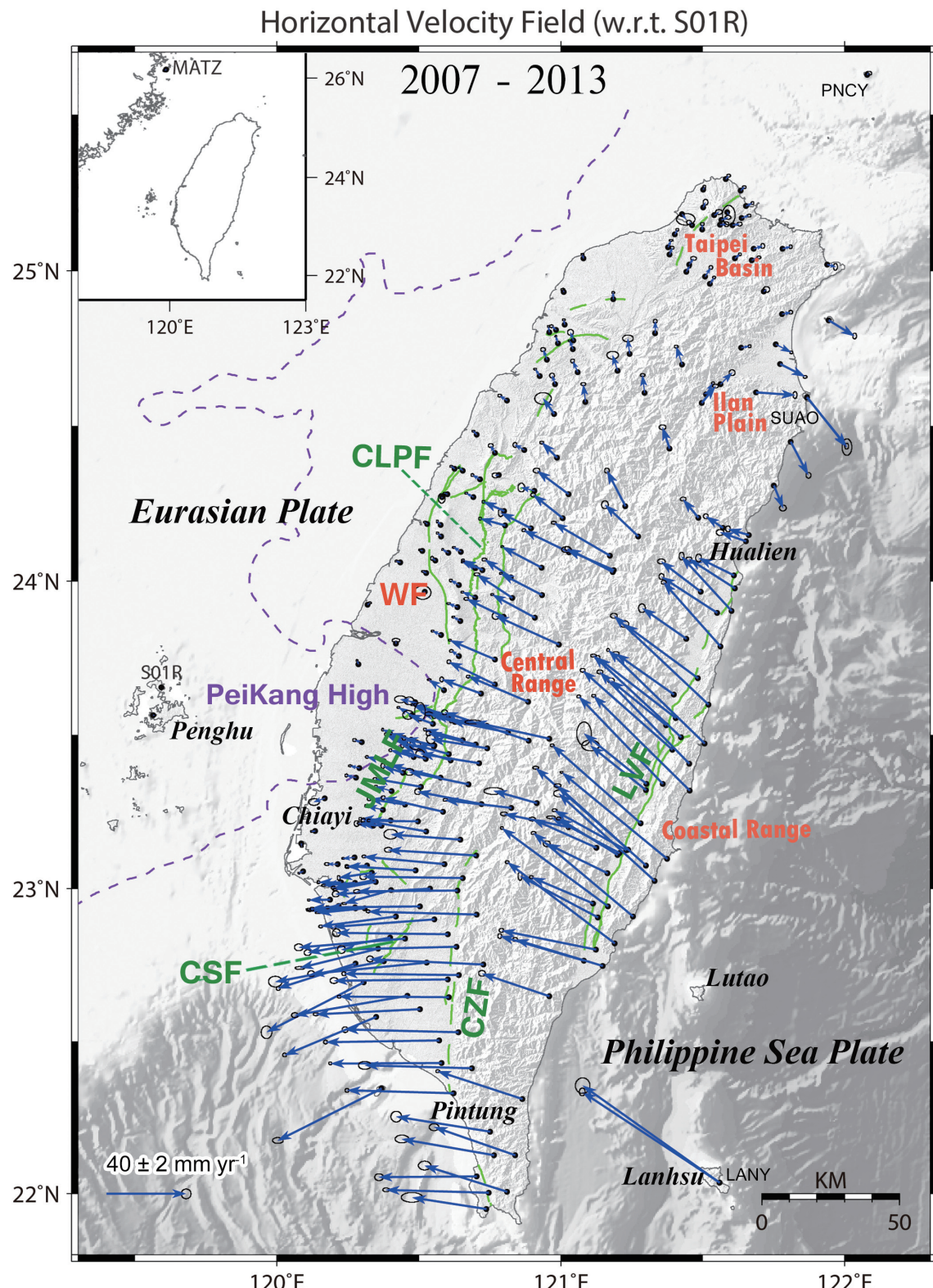


Fig. 21. Horizontal velocities of cGPS stations in the Taiwan area w.r.t. Paisha, Penghu (2007 - 2013). The green lines indicate the surface traces of faults. JMLF, LVF, CSF, CZF, and WF have the same definition as Fig. 19. CLPF denotes the Chelungpu Fault. The blue arrows show velocity vectors. A 95% confidence error ellipse is shown at the tip of each velocity vector. The purple dashed line describes the Peikang High mirage.

sides of JMLF, respectively. Most of the large subsidence sites located at the western Coastal Plain could be caused by groundwater withdrawal (e.g., HUWE). Both the Longitudinal Valley and northern Coastal Range in eastern Taiwan show significant subsidence. In contrast, the southern Coastal Range is uplifting. The rates of uplift and subsidence are about 3 - 11 and 2 - 12 mm yr<sup>-1</sup>, respectively.

Figure 21 shows horizontal velocity field with respect to S01R (Paisha, Penghu) which is located in the Chinese continental margin. The Luzon arc (Coastal Range, Lutao and Lanhsu) is moving northeastward at a rate of about 60 - 84 mm yr<sup>-1</sup>. The velocities in the Coastal Range are in the 307 - 311° directions at a rate about 60 - 69 mm yr<sup>-1</sup>. Across the LVF, a major velocity discontinuity about 20 - 30 mm yr<sup>-1</sup> is observed. The movement direction is slightly changed from NW in the Coastal Range to WNW in the Central Range. Along the eastern side of the LVF the velocity decreases northward from about 68 mm yr<sup>-1</sup> in Taitung to 38 mm yr<sup>-1</sup> in Hualien. A clockwise velocity vector rotation is observed in the Ilan Plain and the velocity reaches its maximal value of 32 mm yr<sup>-1</sup> at SUAO in the 141° direction. The Taipei Basin and surrounding area are relatively stable with minor crustal deformation and the velocities here are about 0 - 5 mm yr<sup>-1</sup>.

Approximately half of the plate convergence rate is accommodated on the fold and thrust belt of western Taiwan. The crustal motion shows nearly westward direction with rates of 35 - 45 mm yr<sup>-1</sup> in the Central Range and decreases to 0 - 5 mm yr<sup>-1</sup> in the Coastal Plain area. A significant velocity change of about 12 - 20 mm yr<sup>-1</sup> is detected across the fold and thrust belt where the JMLF and Chelungpu Fault (CLPF) zones are located. In southern Taiwan the horizontal velocity field becomes more complex. It is about 40 mm yr<sup>-1</sup> in the Chiayi-Tainan area and then slowly increases to about 55 mm yr<sup>-1</sup> in the Kaohsiung-Pingtung area with a counterclockwise velocity vector rotation. Since the ITRF2008 S01R vertical velocity is only 0.5 mm yr<sup>-1</sup>, the relative vertical velocity field pattern with respect to S01R is quite similar to the ITRF2008 vertical velocities, as shown in Fig. 20.

Generally, the relative velocity field from 2007 - 2013 exhibits the characteristics of different stages for the Taiwan collision process from south to north: pre-collisional with rapid and distributed convergence (southern Taiwan), collision and suturing (western-central Taiwan), and post-collisional with collapse and extension (northern-northeastern Taiwan) (Lallemand and Tsien 1997; Shyu et al. 2005). The fan-shaped velocity field (Fig. 21) indicates the ongoing collision is resisted by the Peikang High, a Pre-Miocene basement, which acts as a buttress for advancing thrusts and creates a frontal thrust fault system parallel to the basement margin (Tsan and Keng 1968; Moutherneau and Petit 2003). The velocity vector directions are perpendicular to the deformation front (the thrust and fold belt).

## 7. DISCUSSION AND CONCLUSION

We used GAMIT/GLOBK to process 2007 - 2013 Taiwan cGPS data collected by the CWB, IESAS and CGS from 281 sites. After time series analysis, noise analysis and common-mode error correction, we obtained high precision GPS position time series and velocity fields with more realistic uncertainty.

The GPS position time series is used for velocity estimation and denotes the relationship between the site environment and data quality. Some geophysical signals related to the groundwater variation and seismic activity may be detected. The GPS position time series of the SUCH site (Shuangqi, Taichung) presents obvious periodic signals in the E, N, U components (Fig. 22a) and a scattering of data points changed with time. We found this periodic motion is a non-tectonic signal and is in fact due to the changes in site environment. The SUCH station was established in 2005 and a local government agency kept adding lots of decorations and grew trees nearby during the past few years. Figure 22b shows photos taken in 2007 showing the site environment was fine even with some decorative statues in NE GPS antenna monument direction. However, the site photos taken in 2013 (Fig. 22c) reveal big changes in site environment, with more buildings and trees surrounding the station. These obstructions reduce sky visibility and increase GPS position time series data scattering. Furthermore, the sakura trees next to the sites make sky visibility worse during the flower season, which is the obvious source that causes periodic signals in the SUCH position time series. The other two cGPS sites, CLON (Changlong) and NJOU (Nanzhou), are located in the Pingtung Plain. Both sites show remarkable periodic signals with a similar pattern in the GPS position time series U component (Figs. 23 and 24). These two stations are only about 8 km apart and both located at the footwall of the CZF. Comparing with the water level time series of the Qishan groundwater station (operated by CWB; Fig. 25), the GPS position time series of CLON and NJOU in the U component show similar patterns with the groundwater data. The GPS site displacements and groundwater station levels present a decrease in the first half of the year and increase in the last half of the year. This result indicates a periodic variation in GPS time series in the U component for CLON and NJOU is a seasonal signal affected by groundwater level change.

The general pattern of the newly derived 2007 - 2013 velocity field from the Taiwan cGPS Array is quite similar to that from previous studies (Yu et al. 1997, 1999; Hsu et al. 2009; Lin et al. 2010; Ching et al. 2011). The station density is much larger and spatial coverage is better. This indicates the complexity of tectonic structure in Taiwan. There are two major velocity discontinuities of about 20 - 30 and 12 - 20 mm yr<sup>-1</sup> across LVF in eastern Taiwan and frontal thrust faults in western Taiwan, respectively. In northeastern Taiwan, the velocity vectors reveal a clockwise

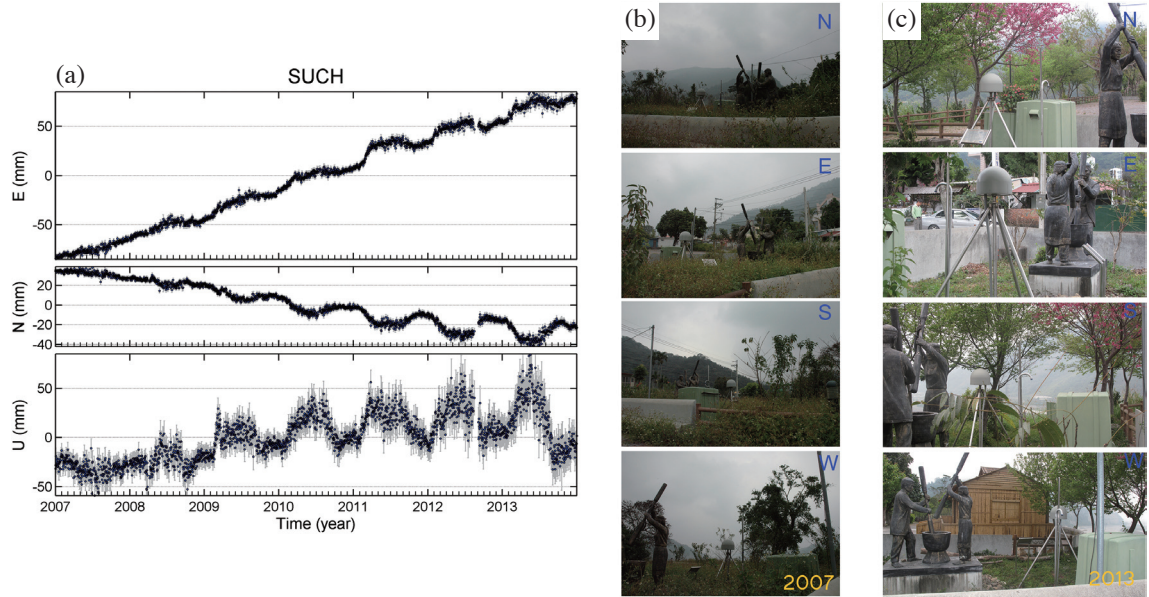


Fig. 22. (a) GPS position time series of SUCH station from 2007 - 2013. (b) and (c) station photos taken in 2007 and 2013, respectively.

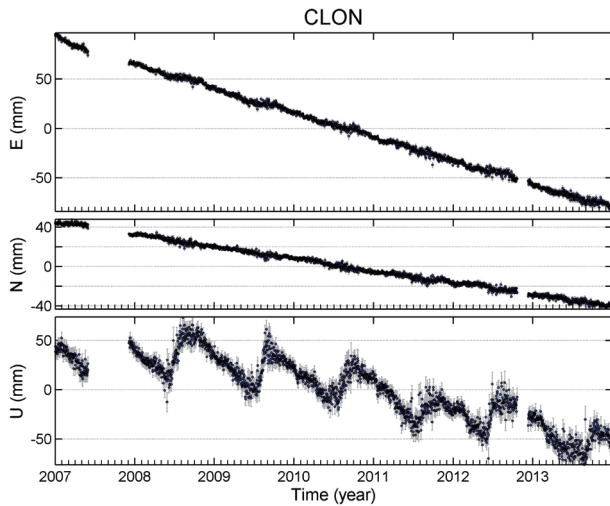


Fig. 23. GPS position time series of CLON station in the east, north and up components, respectively. The black solid circles and light gray bars indicate the observed daily solutions and their formal errors, respectively.

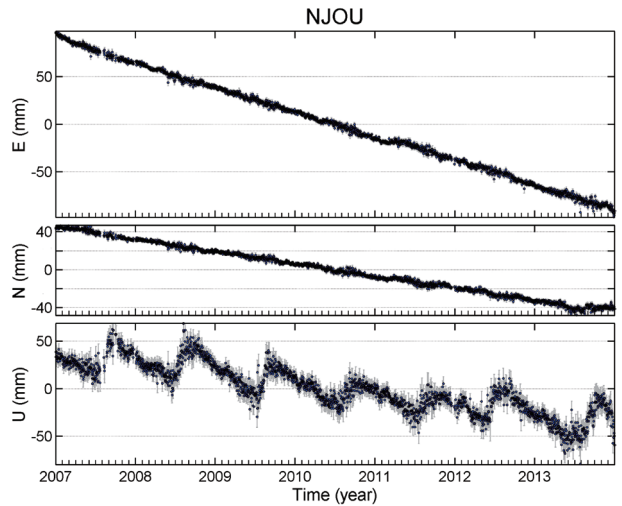


Fig. 24. GPS position time series of NJOU station in the east, north and up components, respectively. The black solid circles and light gray bars indicate the observed daily solutions and their formal errors, respectively.

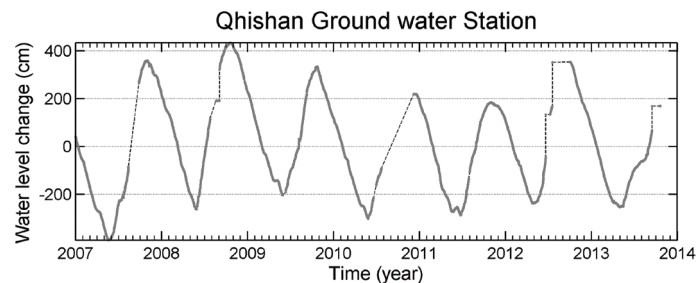


Fig. 25. Groundwater level time series of Qhishan station from 2007 - 2013.

rotation pattern. This indicates the area is undergoing extensional crustal deformation related to the back-arc extension of the Okinawa Trough (Kimura 1985). The velocity of western Taiwan generally shows a fan-shaped pattern, which is consistent with the maximum compression tectonic stress direction inferred from focal mechanisms (Yeh et al. 1991), borehole break-out data (Suppe et al. 1985), and geological strain field (Lee and Wang 1988; Lu et al. 1989; Angelier et al. 1990).

In southern Taiwan the velocities increase southward with the directions becoming southwesterly. It reaches 50 - 55 mm yr<sup>-1</sup> in the Kaoshiung-Pingtung area and deflects about 30° counterclockwise in the direction near the Kaoshiung-Pingtung coast. This movement could be related to tectonic extrusion. Widespread soft sediments and mudstone resulting in plastic deformation may be the reason that rapid crustal deformation but low seismic activity are found in this area.

**Acknowledgements** We are grateful to many colleagues at the Seismological Center, Central Weather Bureau, Central Geological Survey, and Institute of Earth Sciences, Academia Sinica who have participated in maintaining cGPS array and data processing operations. We are indebted to the Institute of Earth Sciences, Academia Sinica (IESAS) and Central Geological Survey (CGS) of Taiwan as well as the International GNSS Service (IGS) community for providing the cGPS data used in this study. GMT-SYSTEM (Wessel et al. 2013) is used to map the data. This study was financially supported by the Central Weather Bureau and Ministry of Science and Technology of Taiwan under grant MOST 103-2116-M-052-004.

## REFERENCES

- Altamimi, Z., P. Sillard, and C. Boucher, 2002: ITRF2000: A new release of the International Terrestrial Reference Frame for earth science applications. *J. Geophys. Res.*, **107**, doi: 10.1029/2001JB000561. [[Link](#)]
- Altamimi, Z., X. Collilieux, and L. Métivier, 2011: ITRF2008: An improved solution of the international terrestrial reference frame. *J. Geodesy*, **85**, 457-473, doi: 10.1007/s00190-011-0444-4. [[Link](#)]
- Angelier, J., 1986: Preface to the special issue on “Geodynamics of the Eurasia\3-Philippine Sea Plate Boundary”. *Tectonophysics*, **125**, IX-X, doi: 10.1016/0040-1951(86)90003-X. [[Link](#)]
- Angelier, J., F. Bergerat, H. T. Chu, W. S. Juang, and C. Y. Lu, 1990: Paleostress analysis as a key to margin extension: The Penghu Islands, South China Sea. *Tectonophysics*, **183**, 161-176, doi: 10.1016/0040-1951(90)90414-4. [[Link](#)]
- Barrier, E. and J. Angelier, 1986: Active collision in eastern Taiwan: The Coastal Range. *Tectonophysics*, **125**, 39-72, doi: 10.1016/0040-1951(86)90006-5. [[Link](#)]
- Bock, Y., 1994: Crustal deformation and earthquakes. *Geotimes*, **39**, 16-18.
- Boehm, J., A. Niell, P. Tregoning, and H. Schuh, 2006: Global Mapping Function (GMF): A new empirical mapping function based on numerical weather model data. *Geophys. Res. Lett.*, **33**, L07304, doi: 10.1029/2005GL025546. [[Link](#)]
- Ching, K. E., R. J. Rau, K. M. Johnson, J. C. Lee, and J. C. Hu, 2011: Present-day kinematics of active mountain building in Taiwan from GPS observations during 1995-2005. *J. Geophys. Res.*, **116**, B09405, doi: 10.1029/2010JB008058. [[Link](#)]
- Dixon, T. H., 1991: An introduction to the global positioning system and some geological applications. *Rev. Geophys.*, **29**, 249-276, doi: 10.1029/91RG00152. [[Link](#)]
- Dong, D., T. A. Herring, and R. W. King, 1998: Estimating regional deformation from a combination of space and terrestrial geodetic data. *J. Geodesy*, **72**, 200-214, doi: 10.1007/s001900050161. [[Link](#)]
- Estey, L. H. and C. M. Meertens, 1999: TEQC: The multi-purpose toolkit for GPS/GLONASS data. *GPS Solut.*, **3**, 42-49, doi: 10.1007/PL00012778. [[Link](#)]
- Feigl, K. L., D. C. Agnew, Y. Bock, D. Dong, A. Donnellan, B. H. Hager, T. A. Herring, D. D. Jackson, T. H. Jordan, R. W. King, S. Larsen, K. M. Larson, M. H. Murray, Z. Shen, and F. H. Webb, 1993: Space geodetic measurement of crustal deformation in central and southern California, 1984-1992. *J. Geophys. Res.*, **98**, 21677-21712, doi: 10.1029/93JB02405. [[Link](#)]
- Hager, B. H., R. W. King, and M. H. Murray, 1991: Measurement of crustal deformation using the Global Positioning System. *Annu. Rev. Earth Planet. Sci.*, **19**, 351-382, doi: 10.1146/annurev.ea.19.050191.002031. [[Link](#)]
- Herring, T. A., R. W. King, and S. C. McClusky, 2010: GLOBK Reference Manual: Global Kalman Filter VLBI and GPS Analysis, Release 10.4. MIT Department of Earth, Atmospheric, and Planetary Sciences, Massachusetts Institute of Technology, Cambridge, M.A., 91 pp.
- Ho, C. S., 1976: Foothill tectonics of Taiwan. *Bull. Geol. Surv. Taiwan*, **25**, 9-28.
- Hsu, Y. J., S. B. Yu, M. Simons, L. C. Kuo, and H. Y. Chen, 2009: Interseismic crustal deformation in the Taiwan plate boundary zone revealed by GPS observations, seismicity, and earthquake focal mechanisms. *Tectonophysics*, **479**, 4-18, doi: 10.1016/j.tecto.2008.11.016. [[Link](#)]
- Huang, C. Y., P. B. Yuan, and S. J. Tsao, 2006: Temporal and spatial records of active arc-continent collision in Taiwan: A synthesis. *Geol. Soc. Am. Bull.*, **118**, 274-288, doi: 10.1130/B25527.1. [[Link](#)]
- Hudnut, K. W., 1995: Earthquake geodesy and hazard monitoring. *Rev. Geophys.*, **33**, 249-255, doi: 10.1029/95RG00406. [[Link](#)]
- Johnson, H. O. and D. C. Agnew, 1995: Monument motion

- and measurements of crustal velocities. *Geophys. Res. Lett.*, **22**, 2905-2908, doi: 10.1029/95GL02661. [[Link](#)]
- Kimura, M., 1985: Back-arc rifting in the Okinawa Trough. *Mar. Petrol. Geol.*, **2**, 222-240, doi: 10.1016/0264-8172(85)90012-1. [[Link](#)]
- Lallemand, S. E. and H. H. Tsien, 1997: An introduction to active collision in Taiwan. *Tectonophysics*, **274**, 1-4, doi: 10.1016/S0040-1951(96)00294-6. [[Link](#)]
- Langbein, J. and H. Johnson, 1997: Correlated errors in geodetic time series: Implications for time-dependent deformation. *J. Geophys. Res.*, **102**, 591-603. doi: 10.1029/96jb02945. [[Link](#)]
- Lee, C. T. and Y. Wang, 1988: Quaternary stress changes in northern Taiwan and their tectonic implication. *Proc. Geol. Soc. China*, **31**, 154-168.
- Lin, K. C., J. C. Hu, K. E. Ching, J. Angelier, R. J. Rau, S. B. Yu, C. H. Tsai, T. C. Shin, and M. H. Huang, 2010: GPS crustal deformation, strain rate, and seismic activity after the 1999 Chi-Chi earthquake in Taiwan. *J. Geophys. Res.*, **115**, B07404, doi: 10.1029/2009JB006417. [[Link](#)]
- Lu, C. Y., L. J. Sun, J. C. Lee, Y. S. Liou, and T. S. Liou, 1989: The shear structures in the Miocene Lushan Formation of the Suao area, eastern Taiwan. *Proc. Geol. Soc. China*, **32**, 121-137.
- Mao, A., C. G. A. Harrison, and T. H. Dixon, 1999: Noise in GPS coordinate time series. *J. Geophys. Res.*, **104**, 2797-2816, doi: 10.1029/1998JB900033. [[Link](#)]
- Mouthereau, F. and C. Petit, 2003: Rheology and strength of the Eurasian continental lithosphere in the foreland of the Taiwan collision belt: Constraints from seismicity, flexure, and structural styles. *J. Geophys. Res.*, **108**, doi: 10.1029/2002JB002098. [[Link](#)]
- Nikolaidis, R., 2002: Observation of geodetic and seismic deformation with the Global Positioning System. Ph.D. Thesis, University of California, San Diego, 249 pp.
- Segall, P. and J. L. Davis, 1997: GPS applications for geodynamics and earthquake studies. *Annu. Rev. Earth Planet. Sci.*, **25**, 301-336, doi: 10.1146/annurev.earth.25.1.301. [[Link](#)]
- Shyu, J. B. H., K. Sieh, Y. G. Chen, 2005: Tandem suturing and disarticulation of the Taiwan orogen revealed by its neotectonic elements. *Earth Planet. Sci. Lett.*, **233**, 167-177, doi: 10.1016/j.epsl.2005.01.018. [[Link](#)]
- Suppe, J., C. T. Hu, and Y. J. Chen, 1985: Present-day stress directions in western Taiwan inferred from borehole elongation. *Petrol. Geol. Taiwan*, **21**, 1-12.
- Tabei, T. and W. L. Amin, 2002: Common-mode errors in the GPS coordinates time series - Application of spatial filtering technique. *J. Geodetic Soc. Japan*, **48**, 229-241, doi: 10.11366/sokuchi1954.48.229. [[Link](#)]
- Tsai, M. C., 2004: GPS time series analysis and modeling studies of crustal deformation in southwestern Taiwan. Master Thesis, National Central University, Taipei, Taiwan, 105 pp. (in Chinese)
- Tsai, M. C., 2013: Interseismic crustal deformation and seismic activity in Southwestern Taiwan. Ph.D. Thesis, National Central University, Taipei, Taiwan, 250 pp. (in Chinese)
- Tsai, M. C., S. Y. Yu, and H. L. Chen, 2007: A block model for the interseismic deformation in the Taiwan arc-continent collision zone. American Geophysical Union, Fall Meeting, San Francisco, Abstract, G12A-06.
- Tsan, S. F. and W. P. Keng, 1968: The Neogene rocks and major structural features of southwestern Taiwan. *Proc. Geol. Soc. China*, **11**, 45-49.
- Wdowinski, S., Y. Bock, J. Zhang, P. Fang, and J. Genrich, 1997: Southern California permanent GPS geodetic array: Spatial filtering of daily positions for estimating coseismic and postseismic displacements induced by the 1992 Landers earthquake. *J. Geophys. Res.*, **102**, 18057-18070, doi: 10.1029/97JB01378. [[Link](#)]
- Wessel, P., W. H. F. Smith, R. Scharroo, J. Luis, and F. Wobbe, 2013: Generic Mapping Tools: Improved version released. *Eos, Trans., AGU*, **94**, 409-410, doi: 10.1002/2013EO450001. [[Link](#)]
- Williams, S. D. P., 2003: The effect of coloured noise on the uncertainties of rates estimated from geodetic time series. *J. Geodesy*, **76**, 483-494, doi: 10.1007/s00190-002-0283-4. [[Link](#)]
- Yeh, Y. H., E. Barrier, C. H. Lin, and J. Angelier, 1991: Stress tensor analysis in the Taiwan area from focal mechanisms of earthquakes. *Tectonophysics*, **200**, 267-280, doi: 10.1016/0040-1951(91)90019-O. [[Link](#)]
- Yu, S. B., H. Y. Chen, and L. C. Kuo, 1997: Velocity field of GPS stations in the Taiwan area. *Tectonophysics*, **274**, 41-59, doi: 10.1016/S0040-1951(96)00297-1. [[Link](#)]
- Yu, S. B., L. C. Kuo, R. S. Punongbayan, and E. G. Ramos, 1999: GPS observation of crustal deformation in the Taiwan-Luzon Region. *Geophys. Res. Lett.*, **26**, 923-926, doi: 10.1029/1999GL900148. [[Link](#)]
- Yu, S. B., Y. J. Hsu, L. C. Kuo, H. Y. Chen, and C. C. Liu, 2003: GPS measurement of postseismic deformation following the 1999 Chi-Chi, Taiwan, earthquake. *J. Geophys. Res.*, **108**, 2520-2539, doi: 10.1029/2003JB002396. [[Link](#)]
- Zhang, J., Y. Bock, H. Johnson, P. Fang, S. Williams, J. Genrich, S. Wdowinski, and J. Behr, 1997: Southern California permanent GPS geodetic array: Error analysis of daily position estimates and site velocities. *J. Geophys. Res.*, **102**, 18035-18055, doi: 10.1029/97JB01380. [[Link](#)]